DOT/FAA/TC-21/53

Federal Aviation Administration
William J. Hughes Technical Center
Aviation Research Division
Atlantic City International Airport
New Jersey 08405

Effects of New Jet Fuel Exposure on Aerospace Composites – Phase 1 Final Report

June 2022

Phase 1 Final Report

U.S. Department of Transportation
Federal Aviation Administration

NOTICE

This report is available at the Federal Aviation Administration William J. Hughes Technical Center's Full-Text Technical Reports page: actlibrary.tc.faa.gov in Adobe Acrobat portable document format (PDF).

Technical Report Documentation Page

1. Report No.	2. Government Accession No.	3. Recipient's Catalog No.
DOT/FAA/TC-21/53		

4. Title and Subtitle	5. Report Date
Effects of New Jet Fuel Exposure on Aerospace Composites - Phase 1 Final Report	June 2022
	6. Performing Organization Code ANG-E281
7. Author(s) Naoufal Harich, Rania Bassou, Hajar Righi, Abhijith Madabhushi, Hasnaa Ouidadi, Dounia Boushab, Thomas Lacy, Charles Pittman, Matthew W. Priddy, and Santanu Kundu	8. Performing Organization Report No. DOT/FAA/TC-21/53
9. Performing Organization Name and Address Mississippi State University, 479-1 Hardy Road, Mississippi State, MS 39762	10. Work Unit No. (TRAIS) 11. Contract or Grant No.
12. Sponsoring Agency Name and Address FAA Seattle Headquarters 2200 S 216th St Des Moines, WA 98198	13. Type of Report and Period Covered Final Report 14. Sponsoring Agency Code AIR-600

15. Supplementary Notes

16. Abstract

Composite materials are increasingly used in the aerospace industry as an alternative to metals, primarily due to their high specific mechanical properties (stiffness, strength, etc.), and tailorability. These materials can be subjected to different types of aeronautical fluids during their lifetime. These composites' exposure to organic fluids such as fuels may lead to matrix swelling and degradation of the composite's material properties. Hence, evaluating property changes as a function of fuel exposure to ensure aircraft flight safety is of paramount importance. A number of alternative jet fuels have come to focus in recent years to reduce the environmental impact of commercial aviation jet fuels. These blended jet fuels are intended to be used as drop-in fuels in aircraft since they meet existing certification limits required of conventional Jet A fuels. The effects of the following jet fuel blends were investigated in this work; 50/50 Gevo Alcohol-to-Jet (ATJ)/Jet A fuel, 50/50 Synthetic Paraffinic Kerosene (SPK)/Jet A, Amyris 20/80 farnesane/Jet A fuel, and 50/50 S8/Jet A. Note that the first three listed fuels are bio-derived, while the latter is derived via natural gas. The objective of this research is to determine the extent of initial fuel absorption in various composites and investigate the effect of such absorption on the composites' glass transition temperature T_g and degradation of composite materials' properties (storage E' and loss moduli E'' and $tan\ \delta$). Specifically, the changes in T_g were identified as a function of the type of fuel, and duration of exposure. The specimens used were autoclave-cured Hexcel SGP370-8H/8552 eight-harness satin weave carbon/epoxy prepreg specimens with two layups: a four-ply [0/-45/+45/90] layup and a four-ply $[0/90]_s$ layup 2 x 0.5 in^2 specimens, oven-cured Jaco Aerospace & Industrial DMS 2436 Type 1 Class 72 multi-axial warp-knit dry carbon fabric infused with API-1078 epoxy with a seven-ply [45/-45/0/90/0/-45/45] layup 2 x 0.5 in^2 specimens, and Oven-cured Cytec T40-800 Cycom® 5215 graphite/epoxy prepreg with $[0]_{30}$ layup 1.5 x 0.5 in^2 specimens. Specimens were vacuum-dried to remove any remaining moisture in the carbon/epoxy specimens before submersion in various fuels. Fuel-exposed specimens were periodically measured during fuel immersion to evaluate mass gain and when fuel uptake saturation occurs. After a final weighing, fuel-saturated specimens were used in dynamic mechanical analysis (DMA) to investigate of fuel absorption effect on composites' T_g and dynamic mechanical properties.

17. Key Words	18. Distribution Statement
Dynamic Mechanical Analysis, jet fuel, glass transition temperature, storage modulus, loss moduli, biofuel, alternative fuel, carbon/epoxy, graphite/epoxy, carbon fiber	This document is available to the U.S. public through the National Technical Information Service (NTIS), Springfield, Virginia 22161. This document is also available from the Federal Aviation Administration William J. Hughes Technical Center at actlibrary.tc.faa.gov.

19. Security Classif. (of this report)	20. Security Classif. (of this page)	21. No. of Pages	22. Price
Unclassified	Unclassified	85	

Form DOT F 1700.7 (8-72) Reproduction of completed page authorized

Contents

Figures

Tables

Acronyms

Acronym	Definition
ASTM	American Society for Testing and Materials
ATAG	Air Transport Action Group
ATJ	Alcohol-to-jet
CAAFI	Commercial Aviation Alternative Fuels Initiative
DMA	Dynamic mechanical analysis
FAA	Federal Aviation Administration
FT	Fischer Tropsch
HEFA	Hydroprocessed esters and fatty acids
HFS-SIP	Hydroprocessed fermented sugars to synthetic iso-paraffins
HRJ	Hydrocracked renewable jet
ILT	Inter-laminar tension
JP	Jet propellant
NCAMP	National Center for Advanced Materials Performance
RH	Relative humidity
SPK	Synthetic paraffinic kerosene

Executive summary

In recent years, there has been a surge in composite materials usage due to several advantages they offer, such as tailorability, higher specific stiffness and strength, and improved fatigue and corrosion resistance. Despite these benefits, composites may exhibit mechanical and thermomechanical property degradation under extreme environmental conditions. Moreover, exposure to and absorption of organic fluids like fuels leads to matrix swelling, which rearranges the polymer molecular conformations and interactions with neighboring polymer segments, motional freedom, and crystallinity. It is, therefore, important to aircraft flight safety that property changes as a function of fuel exposure are evaluated.. In recent years, several alternative jet fuels have been developed to reduce the environmental impact of commercial aviation jet fuels. However, there is still a lack of literature on the impact of alternative jet fuels on composites. These blended jet fuels are intended to be used as drop-in fuels in aircraft since they meet existing certification limits required of conventional Jet A fuels. The effects of the following jet fuel blends were investigated in this work: 50/50 Gevo alcohol-to-jet (ATJ)/Jet A, 50/50 synthetic paraffinic kerosene (SPK)/Jet A, Amyris 20/80 farnesane/Jet A , and 50/50 S8/Jet A. Note that the first three listed fuels are bio-derived, while the latter is derived via natural gas. The objective of this research is to examine the underlying mechanisms behind the storage E' and loss moduli E'', $tan\ (\delta)$ and glass transition temperature T_g degradation of composite materials when exposed to or immersed in Jet A, ATJ/Jet A, SPK/Jet A, S8/Jet A, and farnesane/Jet A fuels. Specifically, the effects of fuel exposure and absorption on T_g are identified as a function of the type of fuel and duration of exposure. Carbon/epoxy and graphite/epoxy specimens were used in this study. Specifically, the following composites were used: autoclave-cured Hexcel SGP370-8H/8552 eight-harness satin weave carbon/epoxy prepreg specimens with a four-ply [0/-45/+45/90] and a four-ply $[0/90]_s$ layup 2 x 0.5 in^2 specimens; oven-cured Jaco Aerospace & Industrial DMS 2436 Type 1 Class 72 multi-axial warp-knit dry carbon fabric infused with API-1078 epoxy with a seven-ply [45/- 45/0/90/0/- 45/45] layup 2 x 0.5 in^2 specimens; and oven-cured Cytec T40-800 Cycom® 5215 graphite/epoxy prepreg with $[0]_{30}$ layup 1.5 x 0.5 in^2 specimens. Vacuum drying was used to remove any remaining moisture in carbon/epoxy and graphite/epoxy specimens before exposing them to the test fuels. Each fuel-exposed specimen was periodically measured during fuel immersion to evaluate mass gain and timing of fuel uptake saturation.. After a final weighing, fuel-saturated specimens were studied by dynamic mechanical analysis (DMA) to investigate the effect of fuel absorption on E', E'', $tan\ \delta$), and T_g. Overall, the fuel uptake and DMA results were well within of currently used Jet A, indicating that the fuel blends used in this study are suitable for use in larger aircraft structures, and perhaps at higher blending ratios.

1 Introduction

1.1 Background and motivation

Composite materials are increasingly employed in the aerospace industry as an alternative to metals, primarily due to their enhanced mechanical properties (stiffness, strength, etc.) and tailorability. These materials have applications in primary aerospace structures such as fuselage, wings, and fuel tanks for general aviation (GA) aircraft, commercial aircraft, and unmanned aerial vehicles. Composite use in aerospace vehicles leads to lower mass, which in turn can lead to improved fuel efficiency. Utilizing fiber-reinforced polymers in aircraft structures can lead to overall weight reductions of 20-40% compared to metallic structures since composites have lower densities than metals (Mazumdar, 2001). In addition, composite structures display exceptional corrosion and fatigue resistance properties.

Composite materials can be subjected to water, fuels, and other types of aeronautical fluids during their lifetime. These fluids can diffuse through the matrix phase, leading to liquid uptake into the composite; however, the amount of diffused fluid depends on the contact timescale as well as other material characteristics (e.g., porosity, resin content, fiber size, etc.). The chemical and physical interactions between the fluid and the matrix also affect the diffusion process. For example, the amount of uptake into a specific matrix of two different aeronautical fluids can vary since the chemical compositions of these two fluids differ. Fluid uptake into polymeric composites (thermoplastics or cured cross-linked resins) can plasticize the matrices and weaken the fiber-to-matrix interface. As a result, the interfacial shear strength will decrease, thus degrading composite properties. This degradation can have a profound effect on the composites' mechanical and thermal properties, potentially leading to premature failure when subjected to mechanical loading.

Compared to the tensile-dominated crack growth in metals, composites display a multitude of failure mechanisms depending on the loading conditions.. For example, when loaded in tension and/or shear, failures are typically caused by matrix cracking, fiber/matrix debonding, delamination, fiber rupture, etc. Stability-related failures such as fiber micro-buckling, face sheet crimping, delamination buckling, and core instabilities under compression loading are also observed. Matrix-dominated and fiber/matrix interface failures can be aggravated as aeronautical fluids diffuse into the matrix and to the fiber/matrix interfaces.

To ensure a deeper understanding of these mechanisms, this report offers a literature review of aeronautical fluids that aerospace fiber/matrix composites and polymers may be exposed to

during their service life (Bassou, et al., 2019). Furthermore, this report investigates the effects of alternative fuel blends and traditional jet fuel immersion on aerospace composites.. Specifically, the report presents the diffusion of these fuels into carbon/epoxy and graphite/epoxy composites. Additionally, it presents the changes in glass transition temperature (T_g) due to fuel absorption as measured by weight using DMA.

1.2 Literature review

The absorption of low-molecular-weight penetrants can significantly affect the matrix-dominated mechanical properties (e.g., compressive strength and compressive modulus) and thermomechanical properties (e.g., T_g) of composites. A common low-weight-molecular penetrant that composites are exposed to is water, in either liquid or water vapor form (e.g., from humid air infusion) (Bond & Smith, 2006). Moisture absorption contributes to matrix swelling, matrix cracking, and matrix plasticization, as shown in Figure 1.

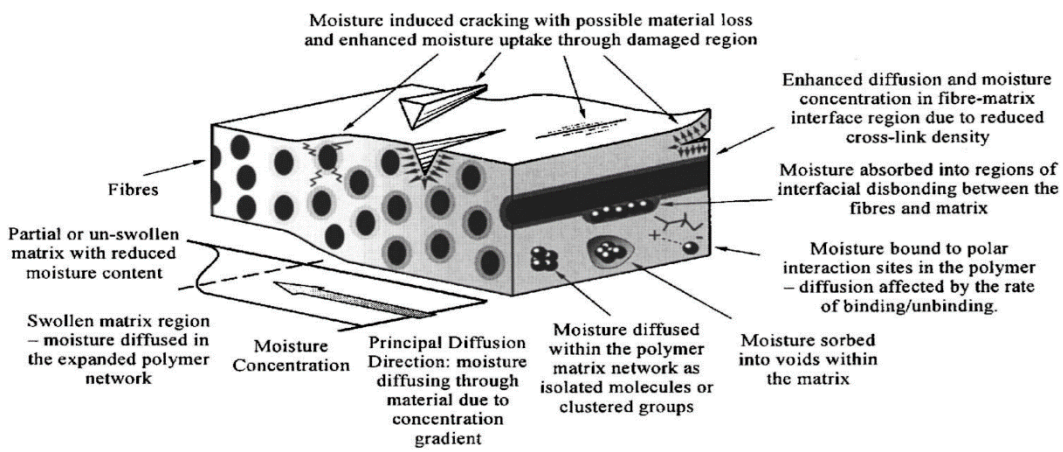

Figure 1. Moisture absorption effects on a composite.

Matrix swelling rearranges the polymer molecular conformations and interactions with neighboring polymer segments. Shrinkage of the matrix relative to the fibers leads to residual stresses. Therefore, moisture-induced swelling will initially decrease residual stress levels. Matrix cracking can occur due to two plausible reasons: moisture-induced swelling stresses are considerably higher than residual stresses, or moisture degrades the fiber/matrix interface sufficiently for the combined thermal swelling residual stress level to induce failure. Fuels, hydraulic fluids, and other low-weight-molecular penetrants have similar effects on aerospace composites' matrices and fiber/matrix interfaces. Matrix swelling and plasticization by water or polar fluids occur due to interchain disruption of polar bond interactions, including hydrogen-bonding disruption, dipole-dipole rearrangements, etc. These changes can degrade composite

mechanical properties when subjected to matrix-dominated loads. Non-polar fuels can solvate non-polar portions of the matrix, disrupting Van der Waals and dispersive interactions. Degradation of the fiber/matrix interface also can occur, which reduces fiber-to-matrix adhesion and load transfer between the matrix and fibers (Bond & Smith, 2006).

Aviation composites can encounter different types of aeronautical fluids during their lifetime. These fluids include anti-icing, hydraulic fluid, aviation fuel, etc. (Ma, Lee, & Tai, 1992). Each fluid will have a unique interaction with the composite or pure polymer (matrix) specimens. This interaction depends on the chemical composition of the fuels or other fluids and the composite matrix (or polymer). Both the fluid and composite matrix chemical compositions control the amount of aeronautical fluid uptake by the composite's matrix (or polymers). One noticeable effect of fluid uptake by composites is swelling. Many studies track weight gain to follow fluid uptake by composites (Curliss & Carlin, 1989; Curliss D. B., 1991). Most aeronautical fluids diffuse into composites faster during the first hours and then slow until reaching a saturation plateau (Curliss & Carlin, 1989; Curliss D. B., 1991). AnFAA Technical Report, DOT/FAA/TC-20/22 (Bassou, et al., 2021) offers a more thorough literature review discussing effects of fluid uptake on composite materials.

2 Materials and fuels used

2.1 Overview of Jet A fuel and alternative fuel blends

Five different fuels were used in this work: one traditional petroleum-based jet fuel (Jet A) and four different blends of alternative jet fuel. The four alternative fuels used are: 50/50 Gevo alcohol-to-jet (ATJ)/Jet A blend, 50/50 synthetic paraffinic kerosene (SPK)/Jet A blend, 20/80 Amyris farnesane/Jet A blend and 50/50 S8/Jet A blend.

2.1.1 Jet A fuel

Jet A is obtained by fractional distillation of crude oil. This fuel is similar to kerosene and consists of hydrocarbons with 8-12 carbon atoms, as shown in Figure 2 (Rahmes, et al., 2009). Some amounts of naphthenic and aromatic compounds are present in addition to linear and branched alkanes. Gasoline and diesel have physical properties inadequate for airplanes, as the shorter hydrocarbons in gasoline can cause it to be too volatile. The longer hydrocarbons in diesel can increase the fuel's freezing point, constraining the operating conditions of the aircraft (Fellet, 2016).

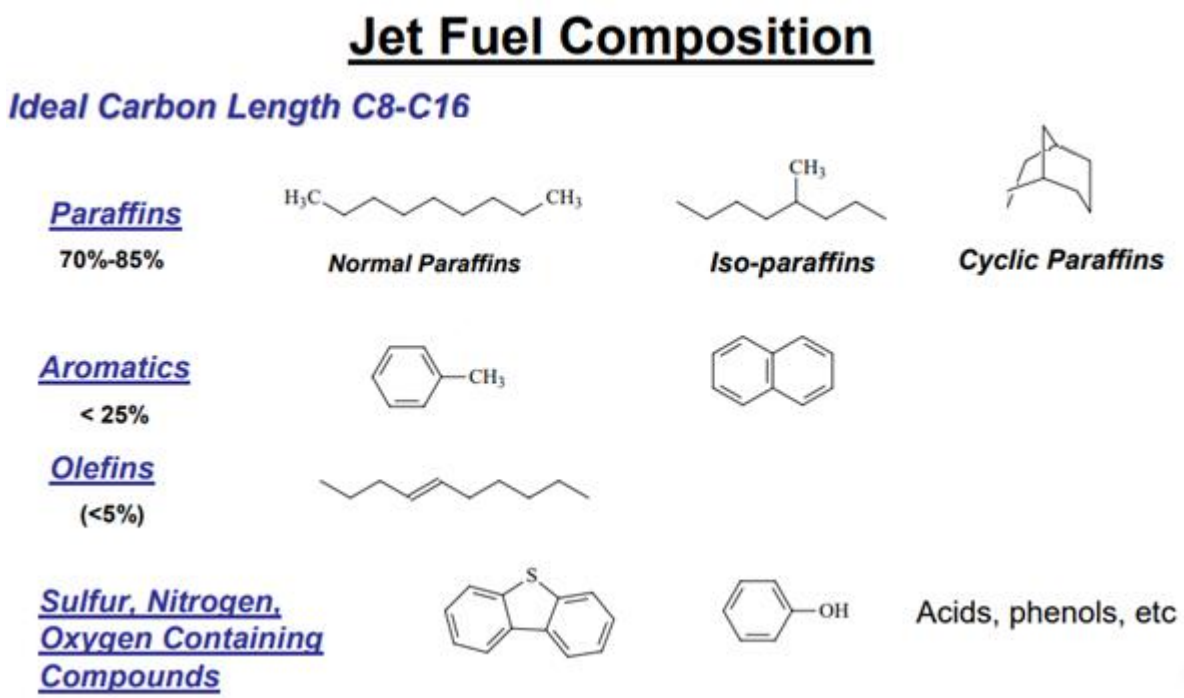

Figure 2. Typical chemical compositions of Bio-SPK and Jet A fuel blends.

Jet A is mostly used in the contiguous United States and some parts of Canada. This fuel has low volatility, with a flashpoint around 38°C and a freezing point of -40°C (Aviation Maintenance Technician Handook - Airframe, 2018). Table 1 illustrates the overall weight % content of the n-paraffin, iso-paraffin, olefin, naphthene, and aromatic fractions, along with a list of Jet A fuel properties (Pires, Han, Kramlich, & Garcia-Perez, 2018).

Table 1. Jet A fuel chemical components, their %weight content, and the fuel's properties.

Jet A fuel chemical components	**Chemical component % weight content**	**Jet A fuel properties**	
n-Paraffin	28.1%	Flash point	38°C (100°F)
Iso-paraffin	38.8	Freezing point	-40°C (-40°F)
Olefin	1.2	Density at 15°C (59°F)	0.820 kg/L (6.84 lbm/US gal)
Naphthene	15.1		
Aromatic	14.4		

2.1.2 50/50 Gevo ATJ /Jet A blend

ATJ fuel from Gevo is a non-fossil-based alternative jet fuel available for commercial use. ATJ is obtained from the ATJ-SPK process. This process was approved in 2016 for use with

conventional jet fuel with a blending ratio of 30% which has been increased to 50% in 2018. Per Air Transport Action Group (ATAG), his process, illustrated in Figure 3 (ATAG, 2009), uses the fermentation of cellulose and sugar feedstock, e.g., sugar cane, sugar beet, hydrolyzed corn/wheat grain starch, and hydrolyzed polysaccharides derived from lignocellulosic biomass (ATAG, 2009).

Numerous bacteria, yeasts, or microbes are utilized to process waste from agricultural products (crop straws, grasses, forestry waste) to be converted to jet fuel either directly or through a number of alcohol conversion pathways. Feedstocks necessary for this process can be easily obtained at a cheaper cost; converting them to fuel does not necessitate much energy, making this process an efficient one (CAAFI Frequently Asked Questions, n.d.; AOPA, 2016; New alternative jet fuel approved., 2016). Both the ATJ-SPK and hydroprocessed fermented sugars (HFS) to synthetic iso-paraffins (SIP) processes are based on the fermentation of sugars to hydrocarbons. The main difference between the two processes remains that unlike the ATJ-SPK process, which generates ethanol, HFS-SIP produces substances such as farnesene. The initial version of the annex issued in 2016 was limited to isobutanol as the feedstock. In 2018, the annex was revised to add ethanol as a feedstock. ATJ Gevo fuel properties are listed in Table 2 below (Pires, Han, Kramlich, & Garcia-Perez, 2018). In the work performed in sections 3 and 4, ATJ is blended with conventional Jet A fuel at 50% by volume.

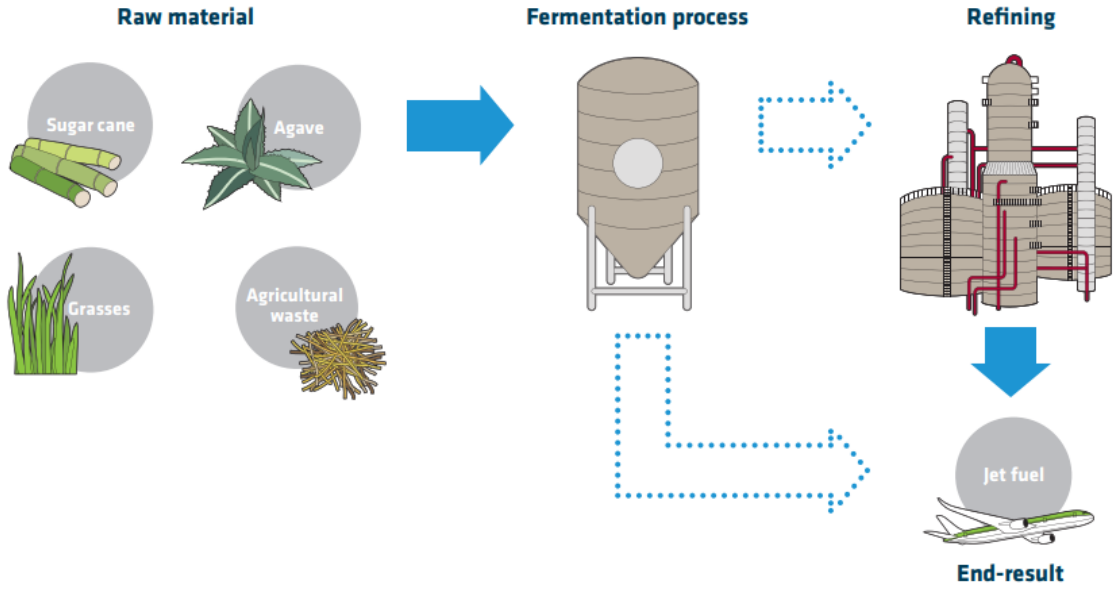

Figure 3. Alcohol-to-jet (ATJ) fuel production process.

Table 2. ATJ Gevo fuel properties (Pires, Han, Kramlich, & Garcia-Perez, 2018).

ATG Gevo fuel chemical components	**Chemical component % weight content**	**ATJ Gevo fuel properties**	
n-Paraffin % weight content	0%	Flash point	45-50°C (113-122°F)
Iso-paraffin % weight content	99.8%	Freezing point	< -78°C (-108.4°F)
Olefin% weight content	0%	Density at 15°C (59°F)	0.76 kg/L (6.34 lb_m/US gal)
Naphthene % weight content	0.2%		
Aromatic % weight content	0%		

2.1.3 50/50 SPK /Jet A blend

Bio-derived SPK is a renewable fuel obtained through the hydroprocessed esters and fatty acids (HEFA) to SPK (HEFA-SPK) process (ATAG, 2009), as shown in Figure 4 (ATAG, 2009).

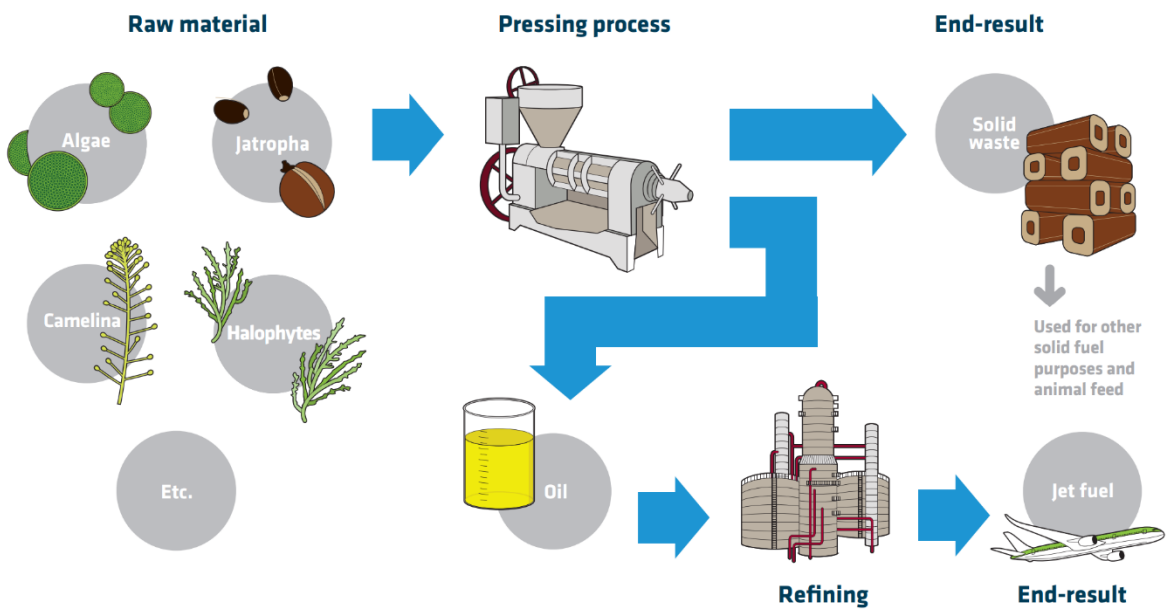

Figure 4. Production of jet fuel through the HEFA-SPK process.

HEFA-SPK fuel is a type of SPK fuel made from bio-based oil feedstocks. The four preferable feedstock sources are jatropha, camelina, algae, and tallow (Pond & Company, Inc., 2012). The terms hydrocracked renewable jet (HRJ), and Bio-SPK have been used to refer to HEFA, but all rely on hydroprocessing as the key step in the conversion process. In hydroprocessing, a feedstock reacts with hydrogen at high pressure and temperatures over a catalyst. The process leads to medium-length (9 to 16 carbon atoms) straight-chain hydrocarbon molecules that are completely saturated. Chemically, the novelty in HEFA/HRJ jet fuel resides in the absence of both aromatics and impurities, and a minimum amount of cycloparaffins (Pond & Company, Inc., 2012). The absence of sulfur, along with a decrease in the maximum size of hydrocarbons used in the combustion process, lead to cleaner emissions.

Distillation is used to separate products derived from crude oil into different types of fuels (diesel, jet, gasoline, etc.). Depending on various parameters, such as distillation techniques, the molecular structure of all the isomers within the boiling range, etc., the product can have different properties suited to their intended use. However, unlike crude oil, the feedstock for HEFA/HRJ must be hydroprocessed before it can be distilled to reduce the number of triglycerides and other impurities. Triglycerides are a class of triesters formed from three fatty acids and glycerol. Some of the impurities present in feedstock are oxygen, nitrogen, and sulfur (Pond & Company, Inc., 2012).

Hydroprocessing consists of deoxygenation and hydrocracking and its aim is to reduce the triglycerides to single-chain hydrocarbons and removing feedstock impurities. These processes eliminate ±90% of these impurities in the HEFA/HRJ feedstock using standard oil cleaning procedures (Pond & Company, Inc., 2012). The oils are then converted to shorter chain diesel-range paraffins through deoxygenation, i.e., the elimination of oxygen molecules from the oil and conversion of olefins to paraffins by adding hydrogen as a reactant. The elimination of oxygen increases the fuel's heat of combustion. The elimination of the olefins and the lack of heteroatoms (O, N, S) increases the fuel's thermal stability (Pond & Company, Inc., 2012; Rahmes, et al., 2009). Consequently, the resulting fuel has a higher combustion heat and greater thermal stability than conventional jet fuel. The hydrogen is pressurized in a catalytic reactor and heated to 316-427°C. After deoxygenation, selective cracking/isomerization occurs, as seen in Figure 5 (Rahmes, et al., 2009), where diesel range paraffins are cracked to mainly branched jet-fuel range paraffins, thus improving the freezing point.

Figure 5. The bio-derived oil-to-SPK conversion process.

Upon hydrocracking completion, the resulting hydrocarbon paraffin mixture is distilled and processed similarly to Jet A-1 or Jet Propellant (JP)-8. Hydrocracking is most efficient when it occurs before distillation so that the impurities do not interfere with subsequent subprocesses (Pond & Company, Inc., 2012; Rahmes, et al., 2009).

Since hydrocracking processes do not generate aromatic compounds that are commonly present in up to 25% in volume in regular jet fuel, a 50% blending ratio of HEFA/HRJ with regular jet fuel is needed to meet the following American Society for Testing and Materials (ASTM) standards: D4054, the "Standard Practice for Qualification and Approval of New Aviation Turbine Fuels and Fuel Additives" (ASTM International, 2020), and D7566 "Standard Specification for Aviation Turbine Fuel Containing Synthesized Hydrocarbons" (ASTM International, 2021). Additionally, this bioderived fuel blend needs to meet the current aviation turbine fuel specification requirements, namely: ASTM D1655 20c (Standard Specification for Aviation Turbine Fuels) (ASTM International, 2020), DEFSTAN 91-091 (The Defense Standard for Turbine Fuel, Kerosene Type, Jet A-1) (Defense Standard, 2019), and the military JP-8 specification for numerous fuel properties such as density (Rahmes, et al., 2009). The resulting HEFA/HRJ is made of molecules which already exist in conventional jet fuel. The resulting HEFA/HRJ product depends on the processing conditions and is mostly independent of the bio-derived feedstock source (Rahmes, et al., 2009). In the work performed in sections 3 and 4, HRJ -a specific form of bio-derived SPK- is blended at 50% by volume with Jet A fuel. Properties of SPK are seen in Table 3.

Table 3. Shell SPK fuel properties (Edwards, Shafer, & Klein, 2012; Pires, Han, Kramlich, & Garcia-Perez, 2018).

SPK fuel chemical components	**Chemical component % weight content**	**SPK fuel properties**	
Aromatic % weight content	0-0.4%	Flash point	>38°C (100°F)
n-Paraffin % weight content	44.9%	Freezing point	< -47°C (-52.6°F)
Iso-paraffin % weight content	55.%	Density at 15°C (59°F)	0.775- 0.840 kg/L (6.47-7.01 lb_m/US gal)

2.1.4 20/80 Amyris Farnesane/Jet A blend

Renewable Farnesane is developed by Total/Amyris and is obtained through the HFS-SIP process (Quignard, 2016). The HFS-SIP process (formerly called Direct-Sugar-to-Hydrocarbon (DSHC)) was approved in 2014 for use with a blending ratio of 10% with conventional jet fuel. This process was developed under ASTM D7566 Annex A3 and was issued in June 2014. The development of this pathway was led by Amyris which has a biorefinery in Brazil's São Paulo area that allows the production of up to 50 000 m^3 of the intermediary product-farnesene- per year while still supplying its renewable diesel product to large areas in Brazil (Quignard, 2016).

The HFS-SIP process, shown in Figure 6 (Quignard, 2016), was originally developed from sugar cane and corn.

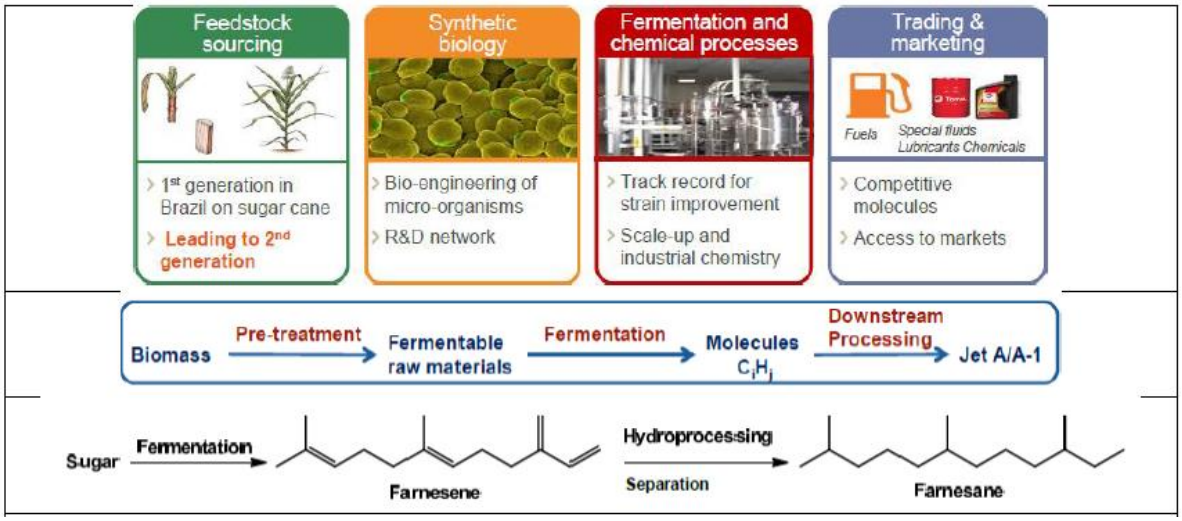

Figure 6. Amyris/Total HFS-SIP ASTM-certified route

Feedstocks consisting of sugars can be straightforwardly treated in the synthetic biologic step with micro-organisms and fermentation reaction. This reaction transforms the carbohydrates to β-farnesene, an iso–C_{15} tetra-olefin (a sesquiterpene molecule 7, 11-dimethyl-3-methylene-1, 6, 10-dodecatriene, chemical formula $C_{15}H_{24}$). Afterward, the olefin is slightly hydrotreated to the corresponding iso-paraffin known as farnesane (2, 6, 10-trimethyldodecane, with chemical formula $C_{15}H_{32}$) that can be straightforwardly used as a base jet-fuel constituent. If the feedstock is the entire biomass, it is necessary to isolate the cellulose and hemicellulose from the lignin as a pretreatment stage. Then hydrolysis converts cellulose to sugars, and fermentation transforms sugars to farnesane (Quignard, 2016). Farnesane is the product of hydrogenation of farnesene. Pure farnesane has a density of 0.77 kg/l, a static viscosity of 3.53 mm^2/s, and a flash point of 110°C. SIP characteristics generally resemble Fischer Tropsch (FT)-SPK and HEFA-SPK, but with the major difference that it is a nearly pure molecule and not a complex mixture of normal and iso-paraffins. In the work performed in sections 3 and 4, farnesane is blended at 20% by volume with Jet A fuel. Table 4 below provides a list of farnesane fuel properties (Quignard, 2016).

Table 4. Farnesane fuel properties (Quignard, 2016).

Farnesane fuel chemical components	**Chemical component % weight content**	**Farnesane fuel properties**	
n-Paraffin % weight content	0%	Flash point	110°C (230°F)
Iso-paraffin % weight content	96.4	Freezing point	< -100°C (-148°F)
Olefin% weight content	0.2	Density at 15°C (59°F)	0.77 kg/l (6.43 lb/US gal)
Naphthene % weight content	1.3		
Aromatic % weight content	0		

2.1.5 50/50 S8/Jet A blend

S8 fuel is an alternative fuel produced by Syntroleum and obtained through the FT-SPK process (ATAG, 2009). The FT-SPK process, illustrated in Figure 7 (ATAG, 2009), was approved in 2009 for use with a blending ratio of 50% with conventional fuels, such as Jet A or Jet A-1 fuels.

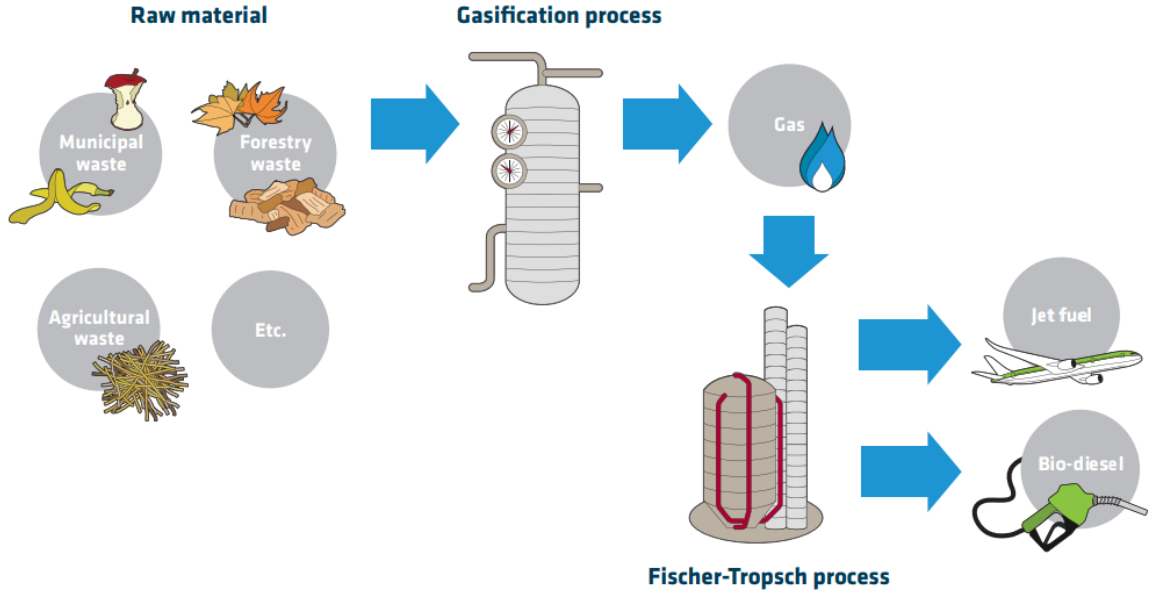

Figure 7. Fuel and bio-diesel production via the FT process

A carbonaceous feedstock source is mainly gasified at high temperatures (1200-1600°C) into carbon monoxide and hydrogen, thus generating syngas. An FT reactor is then used to convert

this syngas into long carbon chain waxes through the FT synthesis. The wax-like product is then cracked and isomerized to develop drop-in fuels similar to the paraffins in petroleum-based jet fuels, but without aromatic compounds. The FT-SPK process combines multiple catalytic processes using cobalt or iron-based catalysts contingent on the synthesis temperature and the goal end products, *e.g.*, jet fuel, biodiesel, gasoline, olefins, or paraffins. Preferably, FT-SPK feedstocks would contain large concentrations of carbon and hydrogen to boost the effectiveness of the thermochemical FT process. Common suitable feedstock are biomass like forestry products or grasses. Biomass is renewable but often varies in carbon content. A less frequently used, yet still renewable, feedstock source is biogas generated from anaerobic digestion of organic matter, *e.g.*, animal manure, landfills, etc. (Biofuels for Aviation: Technology Brief, 2017; CAAFI Frequently Asked Questions, n.d.; Fellet, 2016). S8 is not currently considered a bio-derived alternative jet fuel because the benzene stream is extracted from natural gas, which is a fossil-derived carbon source. In this work, S8 is blended at 50% by volume with Jet A fuel. A list of S8 fuel properties can be seen in Table 5 below (Soloiu, Muinos, Harp, Naes, & Gaubert, 2016).

Table 5. S8 fuel properties (Soloiu, Muinos, Harp, Naes, & Gaubert, 2016).

S8 fuel chemical components	**Chemical component % weight content**	**S8 fuel properties**	
Aromatic % weight content	<0.2%	Flash point	37.8-51.5°C (100-125°F)
n-Paraffin % weight content	22.12%	Freezing point	< -47°C (-53°F)
Iso-paraffin % weight content	75.88%	Density	0.755 kg/L (6.3 lb_m/US gal)

2.1.6 Comparison between alternative fuel/Jet A blends and Jet A fuel

Some of the hydrocarbons found in petroleum-based jet fuels, such as saturated hydrocarbons, linear, branched, and cyclic paraffins, are also formed in these alternative fuels. Unlike Jet A fuel, which has an aromatic weight content of 14.4%, these fuels have very low aromatic content. Moreover, the sulfur levels are nearly zero. Therefore, the combustion of alternative fuels results in reduced air quality emissions, sulfur oxides, and other air pollutants when compared to the combustion of petroleum-based jet fuels.

These alternative fuels are blended with Jet A fuel in specified amounts to satisfy relevant fuel specifications and prevent any unnecessary recertification or great financial investment in aircraft modifications. These blends are referred to as “drop-in alternative jet fuels”. ASTM

D4054, the “Standard Practice for Qualification and Approval of New Aviation Turbine Fuels and Fuel Additives”, must be met for fuels to be approved as drop-in fuels (ASTM International, 2020). A major goal of this study is to understand fuel effects on composites. This understanding will allow incremental increases in the portion of alternative fuels that can be used in aircrafts in the future. Hence, ATJ, SPK, and S8 are blended at 50% by volume with Jet A fuel, whereas Farnesane is blended at 20% by volume with Jet A fuel. An overview of Jet A fuel and the four alternative fuels is seen in Table 6.

Table 6. Fuel properties comparison.

Fuel Properties	**Jet A**	**ATJ Gevo**	**SPK fuel**	**Amyris Farnesane**	**S8**
Process used to obtain this fuel	Distilled from crude oil	ATJ-SPK process	HEFA-SPK process	HFS-SIP process	FT -SPK process
Aromatic % weight content	14.4%	0%	0-0.4%	0%	<0.2%
Flash point	38°C (100°F)	45-50°C (113-122°F)	>38°C (100°F)	110°C (230°F)	37.8-51.5°C (100-125°F)
Freezing point	-40°C (-40°F)	< -78°C (-108.4°F)	< -47°C (-52.6°F)	< -100°C (-148°F)	< -47°C (-53°F)
Density at 15°C (59°F)	0.820 kg/L (6.84 lb_m/US gal)	0.76 kg/L (6.34 lb_m/US gal)	0.775-0.840 kg/L (6.47-7.01 lb_m/US gal)	0.77 kg/L (6.43 lb_m/US gal)	0.755 kg/L (6.3 lb_m/US gal)

2.2 Description of samples used: fabrication process and procurement of aerospace-grade composites

2.2.1 Autoclave-cured Hexcel SGP370-8H/8552 eight-harness satin weave carbon/epoxy prepreg cross-ply and quasi-isotropic specimens

Two four-ply carbon/epoxy composite panels with symmetric cross-ply $[0/90]_s$ and quasi-isotropic [0/-45/+45/90] layups were fabricated of the Hexcel SGP370-8H/8552 eight harness satin weave carbon/epoxy prepreg. These specimens will be referred to as composites A and B for the rest of this document. Four 24 x 24 in.^{2} plies were stacked on an aluminum plate based on the desired layup. Then, the stacked plies were completely covered with an unperforated release film, extending beyond the layup perimeter by approximately 1in. Next, a breather coat was applied over the surface of the release film to avoid bridging. Afterward, the laminate/assembly was entirely covered with a vacuum bag. Extra vacuum bag material was provided in the setup to prevent bridging in corners prior to application of another aluminum plate. Next, a full vacuum was applied overnight. The setup is shown in Figure 8.

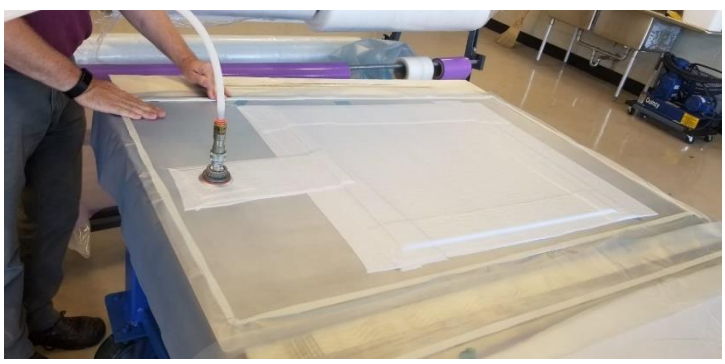

Figure 8. Vacuum bagging of composite A panel.

The Hexcel carbon/epoxy prepreg panels with $[0/90]_s$ and [0/-45/+45/90] layups were autoclave-cured following the temperature and pressure curing cycles shown in Figure 9.

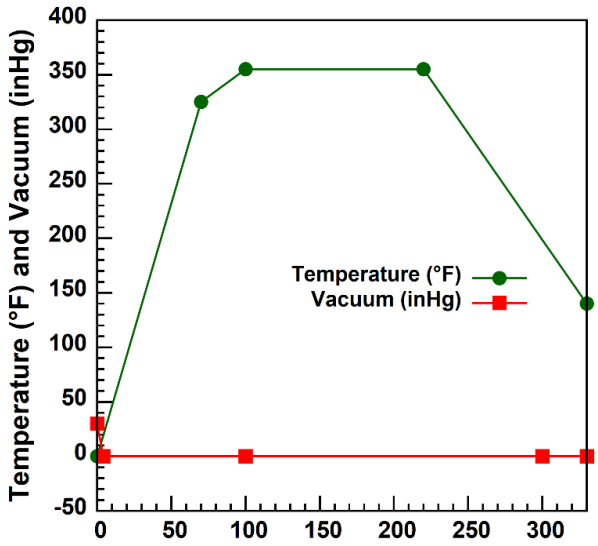

Figure 9. Autoclave-curing cycle used for composite A and B panels.

After curing, the panel had a total thickness of 0.04 in. (1.5 mm) and was cut into 2 x 0.5 in.^{2} specimens, as shown in Figure 10.

Figure 10. A 2 x 0.5 in^2 composite A specimen.

2.2.2 Oven-cured Jaco Aerospace & Industrial DMS 2436 Type 1 Class 72/API-1078 multi-axial warp-knit dry carbon fabric infused with epoxy specimens

Resin-infused panels were obtained from the Advanced Composites Institute (ACI). These panels were made using a Jaco Aerospace & Industrial DMS2436 type 1 class 72 fabric with a [45/-45/0/90/0/-45/45] layup (the areal weight of each ply is shown in Table 7).

Table 7. Ply orientations and the corresponding ply areal weight in composite C panel

Ply Orientation	**Areal Weight**
+45	145 g/m^2
-45	145 g/m^2
0	320 g/m^2
90	145 g/m^2
0	320 g/m^2
-45	145 g/m^2
+45	145 g/m^2

These specimens will be referred to as composite C. One stack of this 7-ply multi-axial warp-knit dry carbon fabric was infused with a standard API-1078 two-part epoxy-amine resin and oven-cured, as seen in Figure 11. The cured resin properties were obtained from the manufacturer: T_g ≈178°C, T_t≈ 191°C. The final fiber/resin content was of 40/60 by volume and 33.33/66.67 by weight.

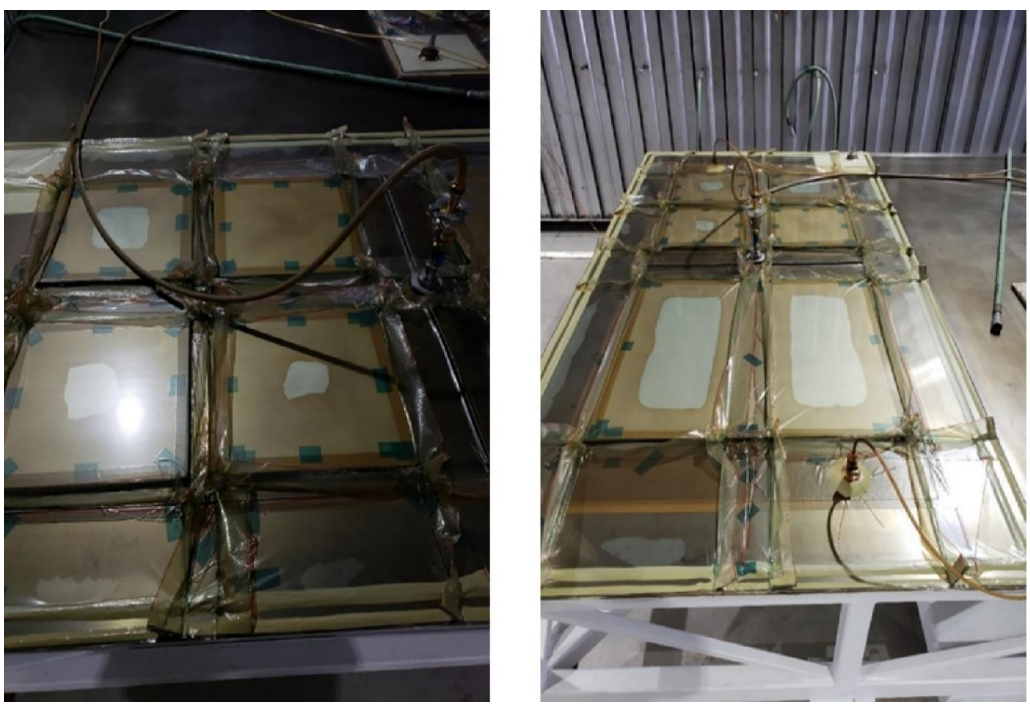

Figure 11. Resin-infusion of a composite C panel.

The panel was cut into 2 x 0.5 in^2 specimens as shown in Figure 12. The final thickness of the panel was of 0.052 in (1.3208 mm).

Figure 12. A 2 x 0.5 in.^{2} composite C specimen.

2.2.3 Oven-cured specimens of a Cytec T40-800 Cycom® 5215 graphite/epoxy prepreg

National Center for Advanced Materials Performance (NCAMP) InterLaminar Tension (ILT) specimens were donated by the National Institute for Aviation Research (NIAR). These ILT specimens were L-shaped Cytec T40-800 Cycom® 5215 graphite/epoxy specimens containing 30 unidirectional plies $[0]_{30}$. These specimens were tested in interlaminar tension under cold temperature dry (CTD) conditions (CTD at -54°, as per ASTM D6415 Interlaminar Tension Standard (ASTM International, 2013)). The L-shaped specimen arms were cut using a water saw. These samples were inspected using an Olympus Omniscan SX flaw detector to ensure no delamination was present in sections located away from the curvature. The samples cut from the L-shaped specimens were then cut again into 1.5 x 0.5 x 0.17 in.^{3} specimens, as seen in Figure 13, to be used for fuel uptake tests and DMA. The Cytec T40-800 Cycom® 5215 graphite/epoxy prepreg used had a resin content of 35% by weight and 45% by volume. These specimens will be designated as composite D.

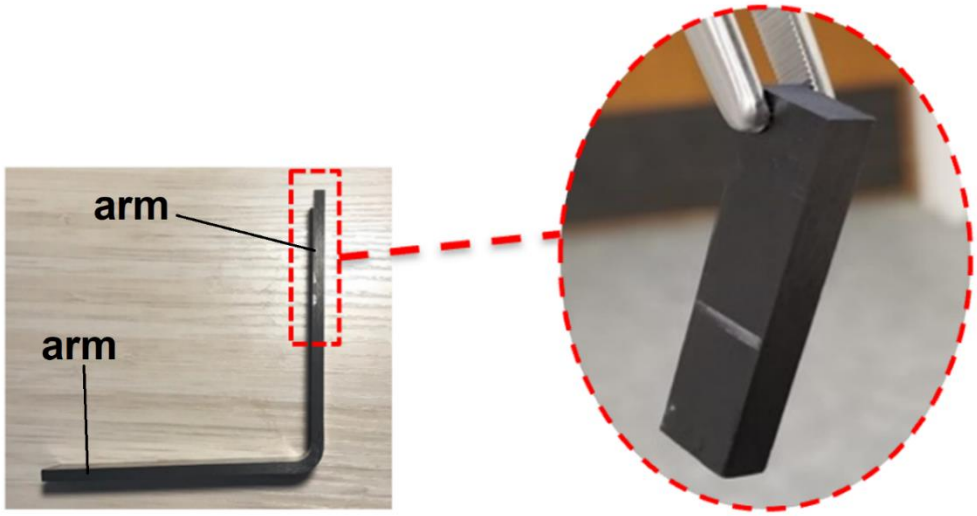

Figure 13. An ILT L-shaped composite D specimen, and a 1.5 x 0.5 in.^{2} specimen cut from one arm.

The cure cycle used for the Cytec graphite/epoxy specimens was cure cycle C described in the "NCAMP Process Specification (NPS) 81323 Rev A" (Figure 14). (Kwan, MacCleod, Ng, & Tomblin, 2007):

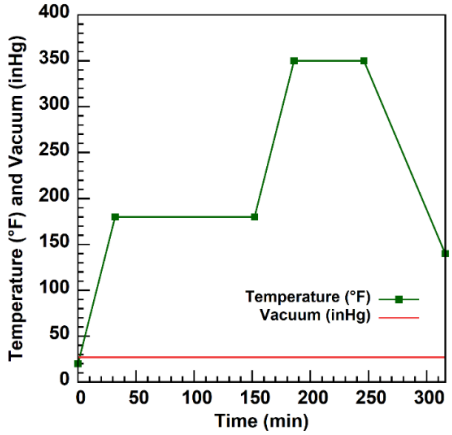

Figure 14. Curing cycle used for composite D specimen.

3 Fuel uptake results of four different carbon/epoxy and graphite/epoxy composites

3.1 Fuel-soaking experiments

Carbon/epoxy 2 x 0.5 in^2 and 1.5 x 0.5 in^2 graphite/epoxy specimens were cut from the different composites mentioned in Section 2.2 using a water saw. These specimens are labeled as A, B, C, and D. Specimens A, B, and C have the same dimensions, whereas specimen D has a slightly shorter length (see Table 8).Three replicates of each specimen except D have been used for the fuel-soaking experiments. The five fuels considered for this study are Jet A and four alternative fuel blends viz. 50/50 Gevo ATJ /Jet A blend, 50/50 SPK /Jet A blend, 20/80 Amyris farnesane/Jet A blend, and 50/50 S8/Jet A blend.

Table 8. Specimen details, dimensions, and the number of replicates for each fuel

Composite specimen	**Specimen size**	**Number of replicates for each fuel**
A: Autoclave-cured Hexcel SGP370-8H/8552 eight-harness satin weave carbon/epoxy prepreg quasi-isotropic with a four-ply [0/-45/+45/90] layup.	2 x 0.5 x 0.06 in^3	3
B: Autoclave-cured Hexcel SGP370-8H/8552 eight-harness satin weave carbon/epoxy prepreg cross-ply with a four-ply $[0/90]_s$ layup.	2 x 0.5 x 0.06 in^3	3
C: Oven-cured Jaco Aerospace & Industrial DMS 2436 Type 1 Class 72 multi-axial warp-knit dry carbon fabric infused with API-1078 epoxy with a seven-ply [45/- 45/0/90/0/-45/45] layup.	2 x 0.5 x 0.05 in^3	3
D: Oven-cured Cytec T40-800 Cycom® 5215 graphite/epoxy prepreg with a $[0]_{30}$ layup.	1.5 x 0.5 x 0.17 in^3	1

The composite specimens were first dried at room temperature using an absolute pressure of 15 inHg (0.5 atm) for at least 12 hours and then held in a controlled humidity chamber at 50% relative humidity (RH) for a minimum of 12 hours before fuel immersion. The specimens were each placed horizontally in separate glass jars containing 100 mL of a specific fuel at room temperature and covered with a screw-on lid, as shown in Figure 15. The glass jars with the samples were stored in a chemical ventilation hood at room temperature during soaking.

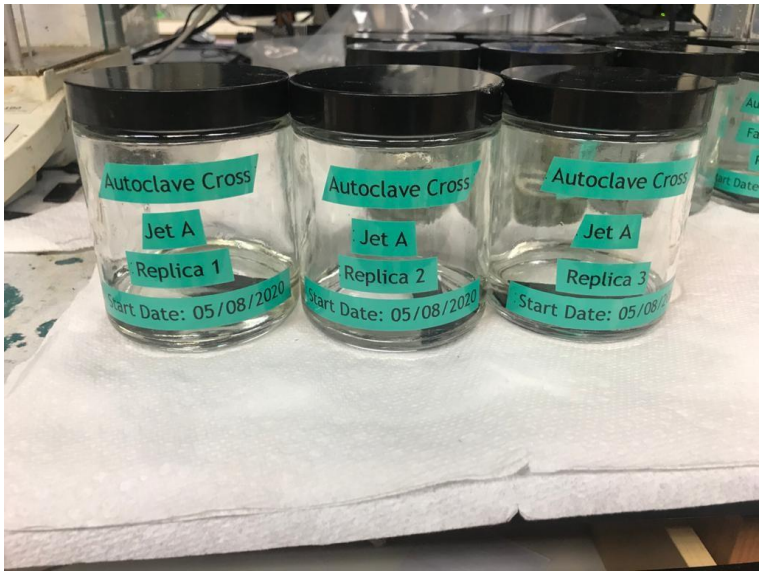

Figure 15. Composite B specimens individually immersed in jars containing 100 mL of fuel.

Fuel-soaked specimens were removed periodically from the glass-jars following the schedule in Table 9, wiped dry, weighed to the nearest 0.1 mg to assess their fluid uptake (as shown in Figure 16), and then re-immersed in the bath. The weight gain due to fuel uptake as a function of immersion time for each specimen and the average fuel-uptake for three replicates in each fuel are reported in this section.

Table 9. Weighing schedule used for the fuel-immersed specimens

Fuel Immersion Time	**Frequency of weighing**
1-8 hours	Every hour
8-24 hours	Every 2 hours
24-36 hours	Every 4 hours
>36 hours	Every 24 hours

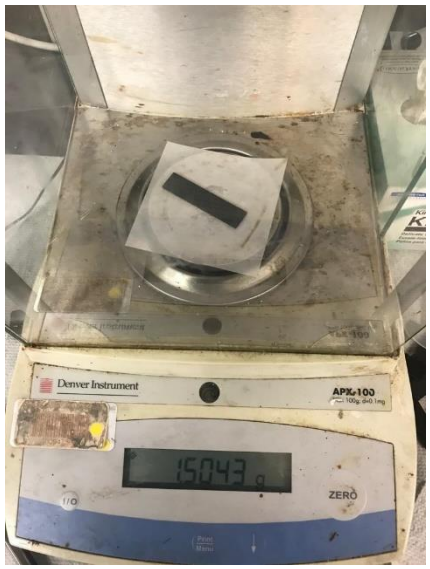

Figure 16. Weighing of a fuel-soaked specimen using a 0.1 mg precision scale.

Each specimen's percentage weight gain was calculated using equation 1, as defined in the ASTM D5229 Moisture Absorption of Matrix Composites standard (ASTM International, 2020). This captures the absorbed amount of fuel over the initial mass of the specimen.

$$\mathrm{WG\%} = (W\_t - W\_i)/W\_i \quad \times\ 100 \tag{1}$$

Where:

- WG% is percentage weight gain, represents the average amount of absorbed fluid in a material.
- W_t is mass of the specimen at a given time t.
- W_i is initial mass of the specimen.

3.2 Overview of fuel uptake by composites

The question that will be addressed in this research is whether alternative fuels can replace standard petroleum-derived jet fuels safely. Current alternative fuels approved for blending with standard jet fuels do not contain aromatic components. In comparison, their petroleum-derived counterparts contain between 8% to 25% aromatic molecules (Moses & Roets, 2009; ASTM International, 2021). This chemical difference might cause different amounts of fuel diffusion into the polymer and composite aircraft components. Fuel diffusion into composites can change the mechanical properties and glass transition temperature of composite structures. Will the differences in fuel composition from blending result in greater diffusion into aerospace-grade

carbon/epoxy or graphite/epoxy composites? Will the mechanical properties of these composites be compromised relative to the use of conventional jet fuels? These questions were studied by immersing four representative composite systems (Table 10) into Jet A fuel and four representative alternative fuels (section 2.1) for 900 hours. Specifically, equilibrium fuel uptake and rate of fuel uptake into the test composites were determined. This provided 20 comparison datasets.. Following this, dynamic mechanical analyses were performed on the neat composite samples and on the same composites after equilibrium fuel uptake was reached in all five test fuels.

Figure 17(A) displays the % weight gain as a function of time for three replicas of composite A and their average submerged in Jet A fluids, whereas the average fuel uptake by these three samples is shown in Figure 17(B).

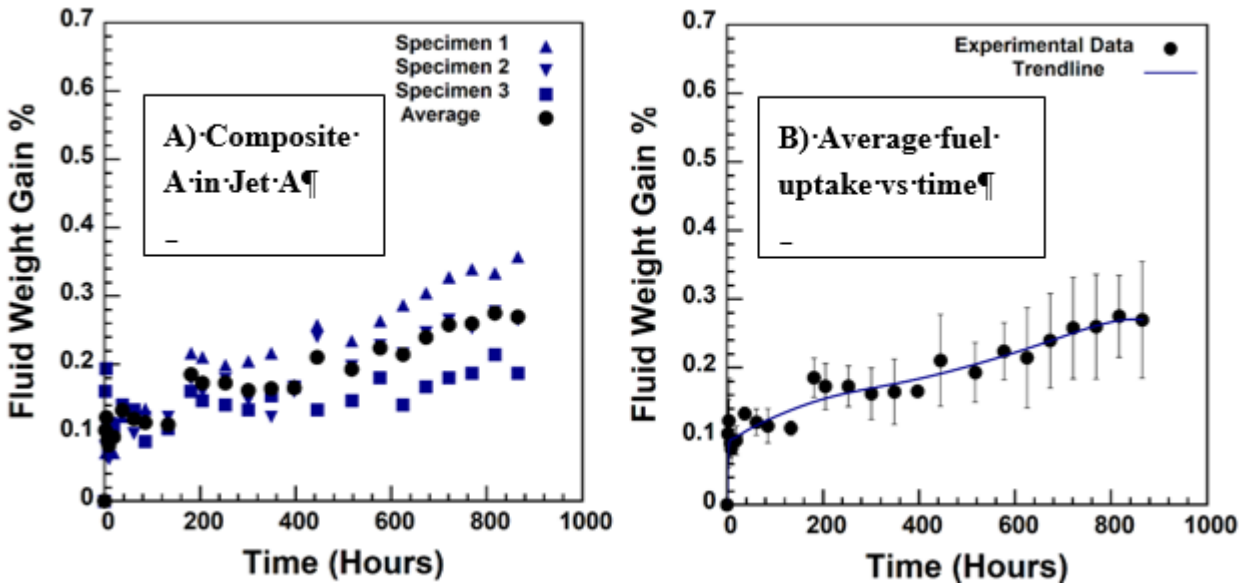

Figure 17. A) Jet A fuel uptake of composite A samples and B) average fuel uptake versus time.

As described below, similar data have been collected for other samples and in different fuels. The absolute magnitude of scatter observed in fuel uptake measurements was low, but the percentage variation was high. This was expected due to the low amounts of fuel absorbed, and the small coupon dimensions used.

The equilibrium uptake is considered to be the final weight gain datapoint collected versus time. The rate of fuel uptake was determined by the tangent to weight gain versus time curves at any specific time. All fuel uptake rates were higher in the first few hours and then decreased. All 20 experiment plots are displayed later in this section for individual examination. Table 10

summarizes the equilibrium weight gains and the experimental variation range (low and high) within the three replicated experiments for each of the four composite systems in all five fuel systems (20 experiments). In this table, the first horizontal row for each composite sample represents final average % fuel uptake value and ± standard deviation. The second row contains the range of final uptake weight % values for three replicates exposed to each fluid.

Table 10. Summary of final average fuel uptake weight % for all specimens and fuels used

Composite Type	**Specimen size**		**Jet A**	**50/50 ATJ/Jet A blend**	**50/50 SPK/Jet A blend**	**20/80 Farnesane/Jet A blend**	**50/50 S8/Jet A blend**
A	2 x 0.5 x 0.06 in^3	Average ± Standard Deviation	0.27% ± 0.08	0.26% ± 0.09	0.3% ± 0.06	0.32% ± 0.04	0.26% ± 0.05
		Range (low-high)	0.18%-0.35%	0.18%-0.35%	0.26%-0.38%	0.28%-0.38%	0.24-0.31%
B	2 x 0.5 x 0.06 in^3	Average ± Standard Deviation	0.28% ± 0.04	0.36% ± 0.13	0.32% ± 0.09	0.29% ± 0.10	0.36% ± 0.04
		Range (low-high)	0.24%-0.34%	0.35%-0.47%	0.18%-0.36%	0.18%-0.38%	0.34%-0.41%
C	2 x 0.5 x 0.05 in^3	Average ± Standard Deviation	0.04% ± 0.01	0.04% ± 0.05	0.05% ± 0.05	0.07% ± 0.03	0.04% ± 0.03
		Range (low-high)	0.03%-0.05%	0.0%-0.06%	-0.09%-0.09%	0.04%- 0.1%	0.02%-0.06%
D	1.5 x 0.5 x 0.17 in^3	Average	-0.01%	-0.05%	-0.05%	0.01%	-0.01%

Statistical analysis was performed on the fuel uptake results obtained during the experiment. The Anova test was used to compare the behavior of each composite type when immersed in each of the five fuels. The results indicate that each type of specimen behaved the same way in the five fuels. In addition, F-test was performed to investigate whether weight gain by a composite specimen in Jet A differs from the other fuels and no statistical difference was observed. In summary, fuel uptake by different composites in Jet A was essentially the same as that in the four alternative fuels blended with Jet A.

The average fuel uptake of three replicas of composite A specimens immersed in all five fuels is shown in Figure 18 (detailed in section 3.3.1).

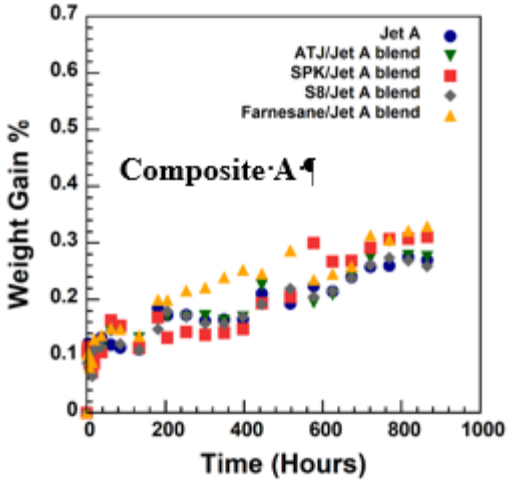

Figure 18. Average fuel uptake by three composite A specimen replicas immersed in different fuels.

To reiterate, all uptake rates were initially higher before converging to similar slower equilibrium weight gains. The low total fuel uptake was expected due to the small specimen dimensions. Different fuel compositions all give similar, very small weight gains. The equilibrium weight gains ranged between 0.26% and 0.32% for Jet A and 20/80 farnesane/Jet A blend. These average fuel uptake results are summarized in Table 10. Composite B displays a similar behavior with an average equilibrium in the range of 0.28% to 0.36% as shown in Figure 19 and are summarized in Section 3.3.2.

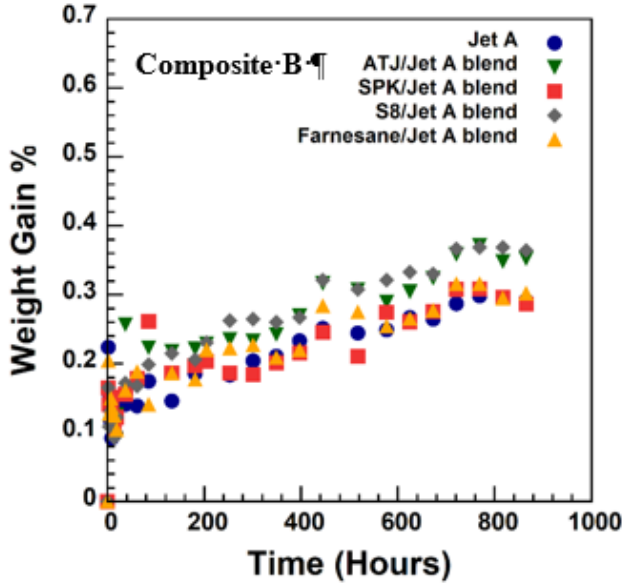

Figure 19. Average fuel uptake by three composite B specimen replicas immersed in different fuels.

The average fuel uptake of three replicas of composite C specimens immersed in all five fuels are shown in Figure 20 and expanded individually in Section 3.3.3.

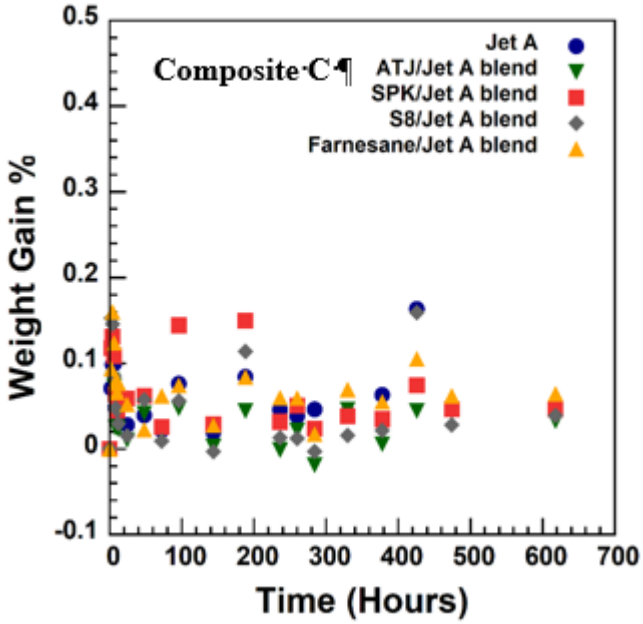

Figure 20. Average fuel uptake by three composite C specimen replicas immersed in different fuels.

All specimens had an initial jump before converging toward an equilibrium value. For composite C the average equilibrium weight-gains ranged from 0.04% to 0.07%. Note, these values are lower than those observed for the composites A and B. See Table 10 for detailed results.

The Cytec graphite/epoxy specimen (composite D) fuel uptake results are presented in Figure 21. The initial increase can be seen for these specimen as well. The equilibrium average ranged from -0.05 to 0.01.

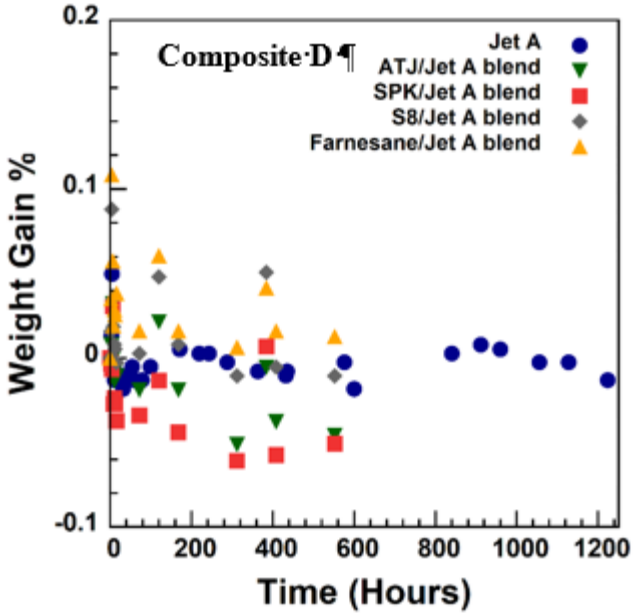

Figure 21. Composite D fuel uptake when immersed in different fuels.

Composite D was significantly thicker (0.17 in.) than samples A-C (0.06 in.). The measured fuel weight gain fluctuated around 0% after immersion in Jet A fuel for 1250 hours, as seen in Figure 22.

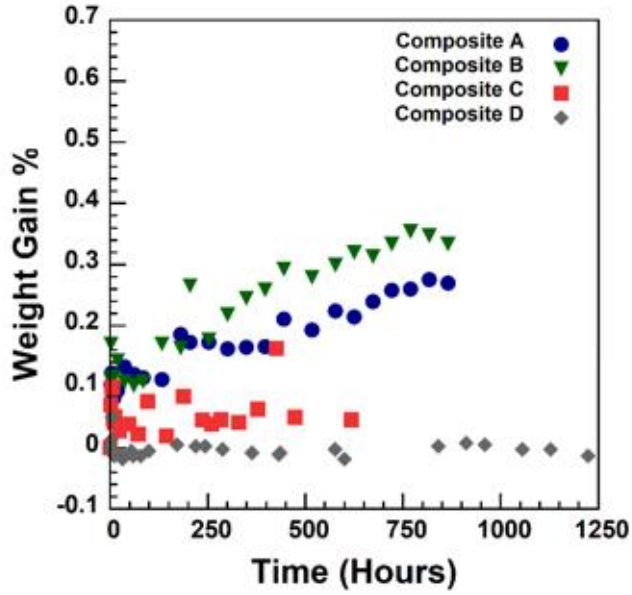

Figure 22. Average fuel uptake by three replicas of composites A, B, and C and one replica of composite D, each immersed separately in Jet A fuel.

The extremely low Jet A fuel absorption for the Cytec graphite/epoxy specimen could mean this specimen's matrix is extremely resistant to fuel diffusion. Alternatively, thicker specimens will take longer to reach uptake equilibrium than samples with the larger surface-to-volume ratios (e.g., thinner samples). If it were to take significantly longer than 1000 hours of fuel immersion to reach equilibrium, this might be a factor. Low equilibrium uptakes by graphite/epoxy samples were also observed for all the fuel blends (Figure 22) when compared to the carbon/epoxy composites. Either or both of the above justifications may explain this negligible weight gain. A final possibility exists for smaller, thinner samples to experience larger fuel uptakes upon immersion. If small cracks, pits, or related flaws intersect the surface, they could take up fuel during immersion. Therefore, samples with high surface-to-volume ratios (e.g., thin samples) could absorb more fuel per unit weight (per unit volume) than thicker, but otherwise identical, samples. The low overall weight gains of the three thin samples (A, B, C) suggests that this possibility did not change any of the overall conclusions reached.

These results led to the following key conclusions:

- Composites A and B show higher weight gain values due to fuel uptake than composites C and D for all type of fuels. This can be explained by the difference in the composite structure (matrix), meaning the matrix used for composites A and B has a better affinity with the fuels used.

- Composite D experienced very low weight gain and displayed weight losses in a few cases. This can be explained if the matrix used for those specimens is resistant to the fuels or if the thickness slows the whole absorption process down (will reach saturation but will take a long time). Degradation of the matrix could lead to weight loss.
- There was no noticeable difference in fuel absorption for specimens immersed in Jet A fuel and alternative fuel blends, regardless of the blending ratio. The final equilibrium fuel-uptake range for all composite specimens immersed in the same fuel, the same fuel by different composites, and by different composites often overlaps. This provides support for permitting the enhancement of the weight fraction allowed of these four alternative fuels if mechanical properties are not adversely impacted relative to Jet A fuel absorption.
- This work indicates that within limits studied, replacing aromatic molecules with aliphatic ones as fuel components, does not cause greater equilibrium fuel diffusion into aerospace grade composites.
- To further establish these points, the following experiments are recommended:
    - Test all four of the alternative fuels at 100 wt (weight) % to determine uptake by the same composites.
    - Prepare Jet A fuel in the same boiling point range enhanced to contain 75 wt % aromatic compounds and perform analogous uptake immersion tests.
    - Perform similar fuel uptake experiments on thicker composite principal structural elements.

3.3 Fuel uptake data for all specimens

This section explains fuel uptake by individual composite specimens when immersed in five different fuels and averaged data with standard deviations and trendlines.

3.3.1 Fuel uptake for composite A

Figure 23 -Figure 27 show composite A specimens immersed separately in each of the five fuels. Please note that the solid line represents Bezier trendlines in Figure 23B -Figure 27B.

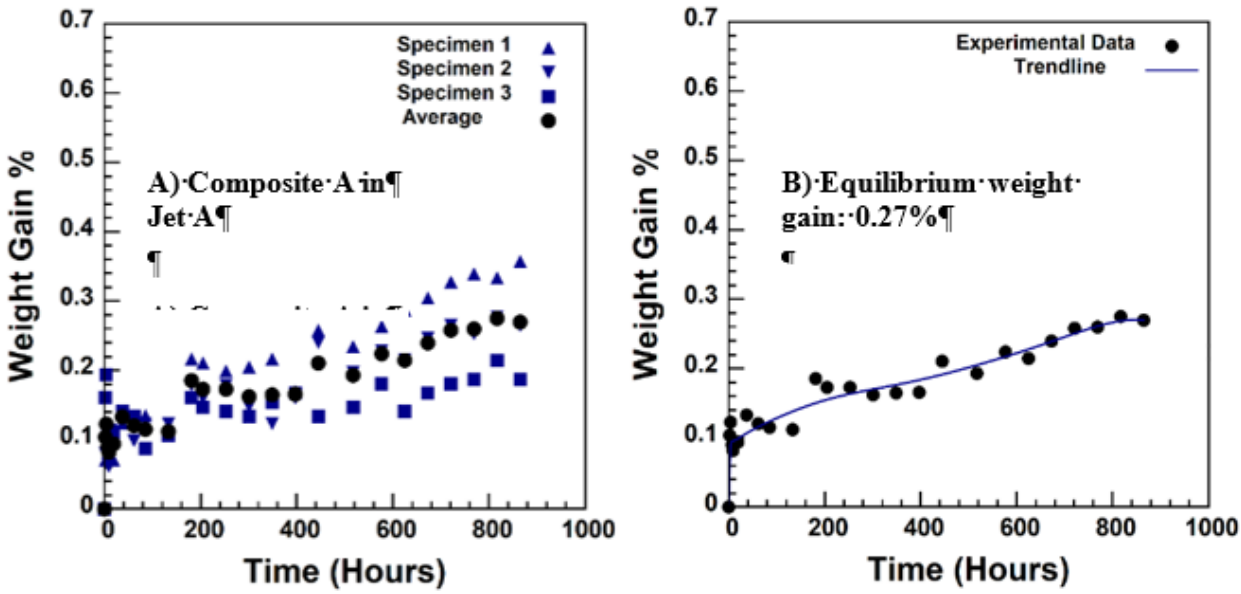

Figure 23. A) Jet A fuel uptake by composite A and B) average fuel uptake versus time.

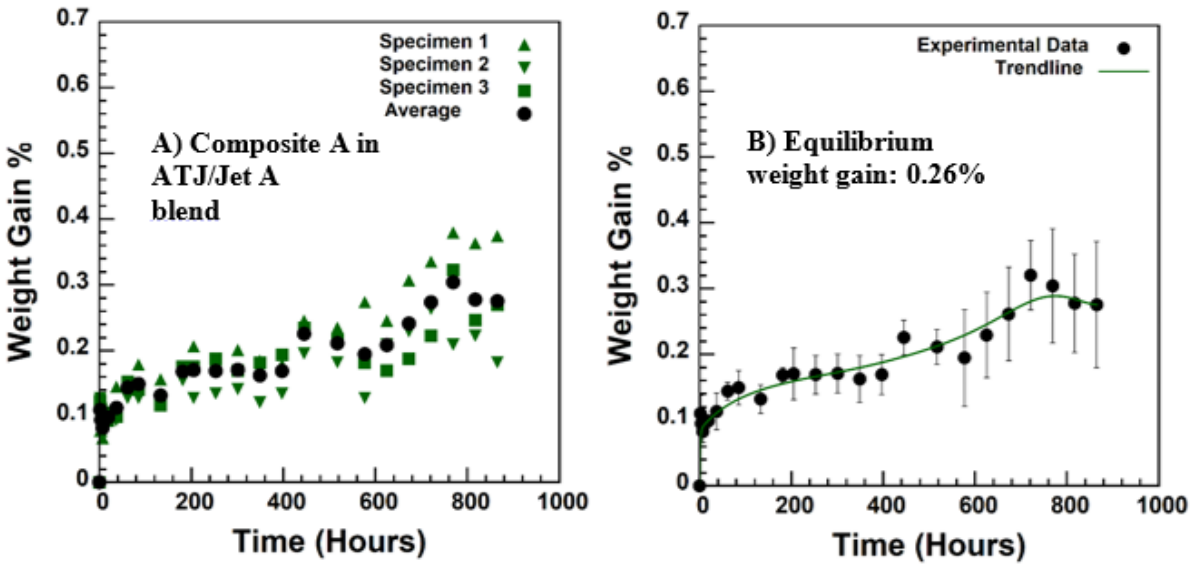

Figure 24. A) Fuel uptake by composite A of ATJ/Jet A blend and (B) average fuel uptake versus time.

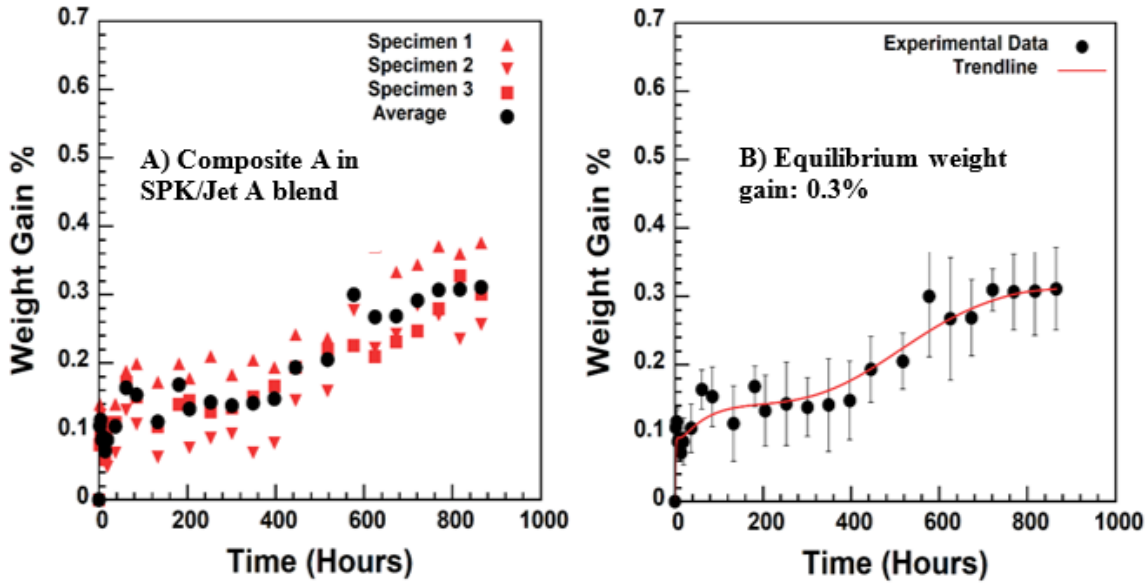

Figure 25. A) Fuel uptake by composite A of SPK/Jet A blend and (B) average fuel uptake versus time.

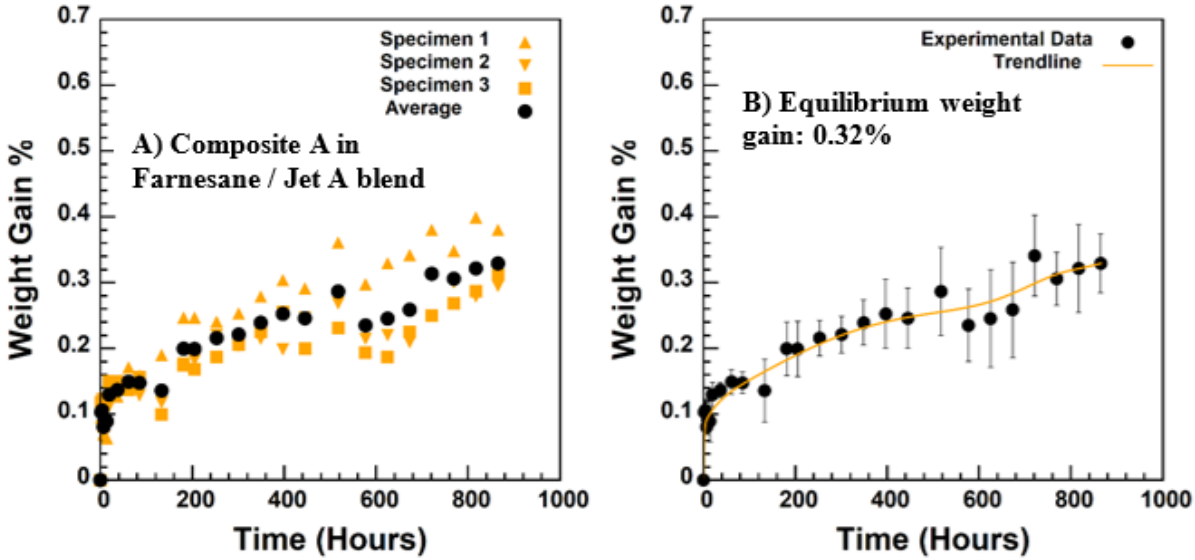

Figure 26. A) Fuel uptake by composite A of Farnesane/Jet A blend and B) average weight gain versus time.

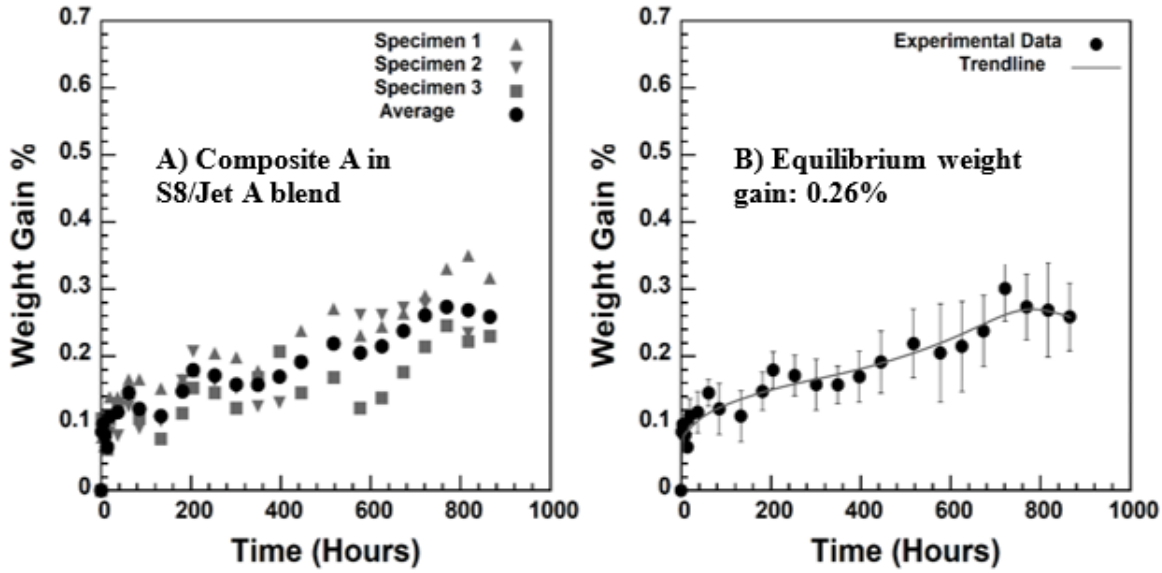

Figure 27. A) Fuel uptake by composite A of S8/Jet A blend and B) average percentage weight gain versus time.

3.3.2 Fuel uptake for composite B

Figure 28 -Figure 32 show composite B specimens immersed separately in each of the five fuels. Please note that the solid line represents Bezier trendlines in Figure 29B -Figure 32B.

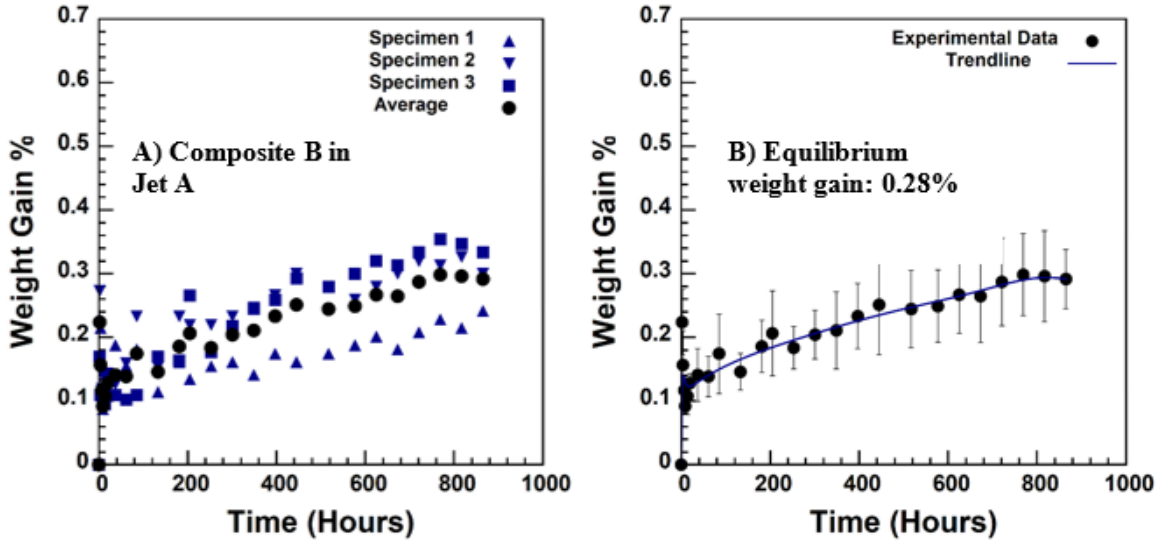

Figure 28. A) Jet A fuel uptake by composite B and B) average percentage weight versus time.

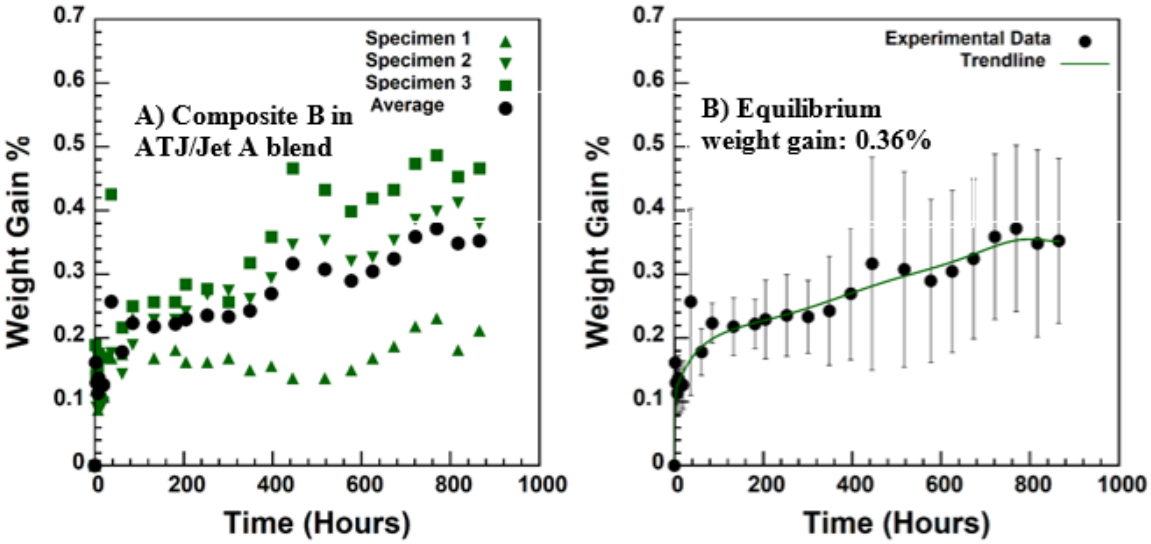

Figure 29. A) Fuel uptake by composite B of ATJ/Jet A blend and B) average weight gain versus time.

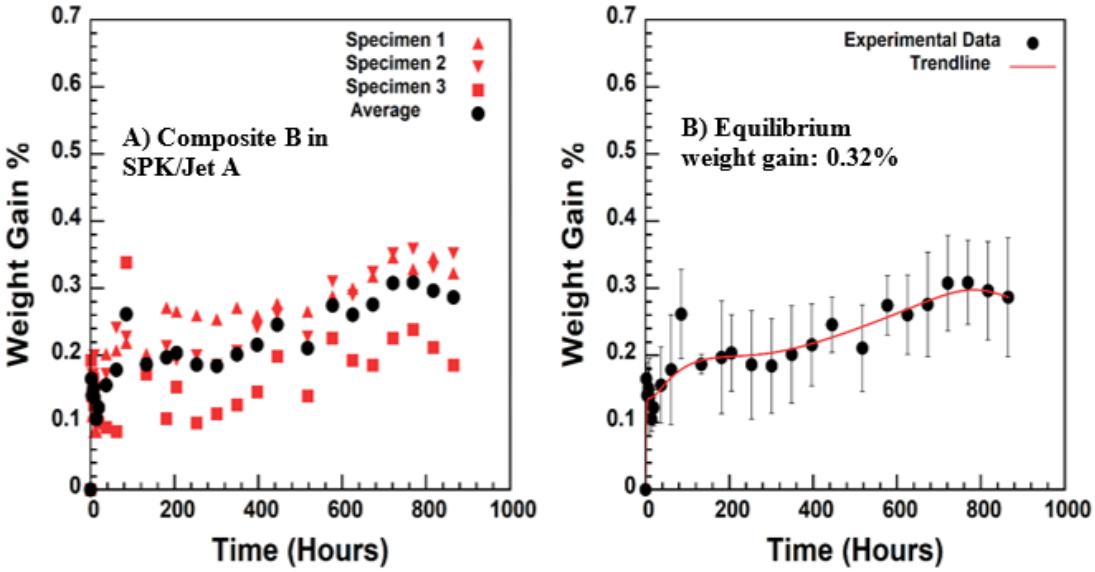

Figure 30. A) Fuel uptake by composite B of SPK/Jet A blend and B) average weight gain versus time.

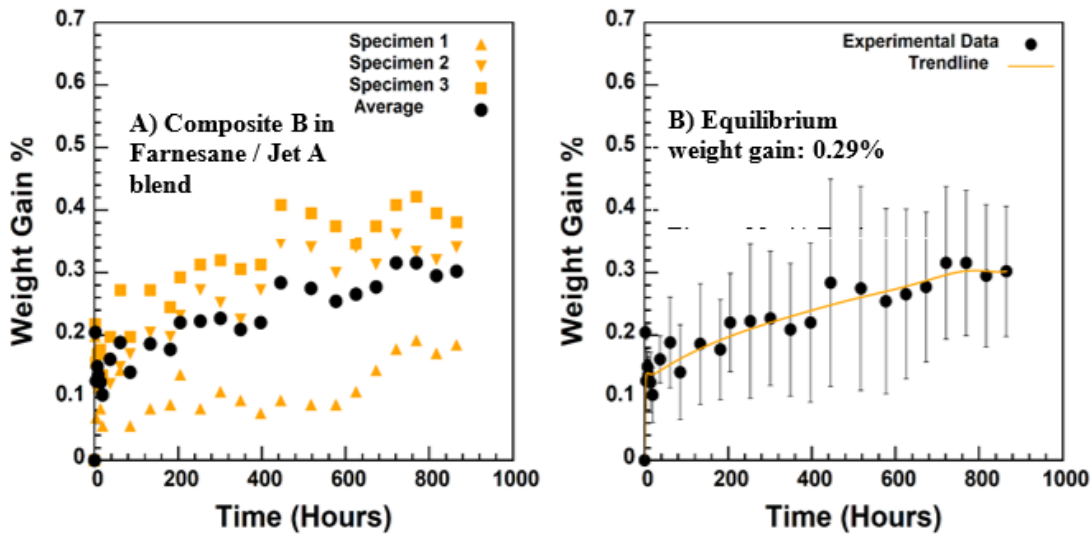

Figure 31. A) Fuel uptake by composite B of Farnesane/Jet A blend fuel and B) average weight gain versus time.

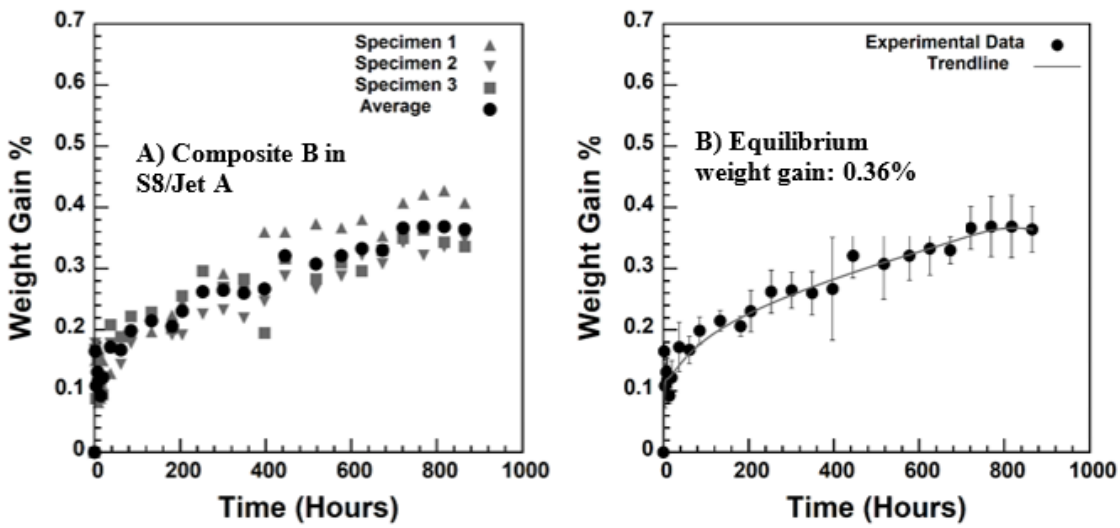

Figure 32. A) Fuel uptake by composite B of S8/Jet A blend and B) average weight gain versus time.

3.3.3 Fuel uptake for composite C

Figure 33 through Figure 37 show composite A specimens immersed separately in each of the five fuels. Please note that the solid line represents Bezier trendlines in Figure 33B through Figure 37B.

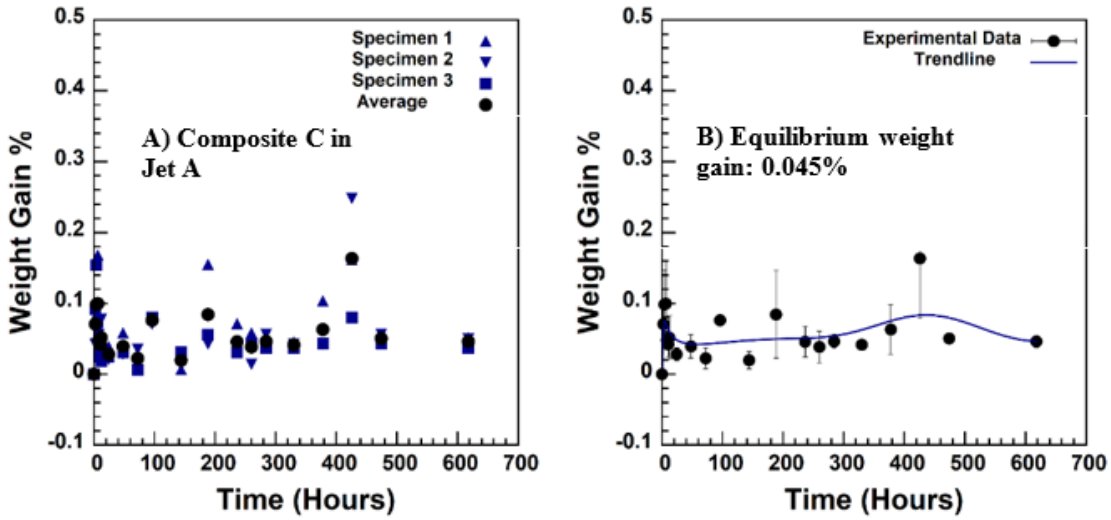

Figure 33. A) Jet A fuel uptake by composite C and B) average weight gain versus time.

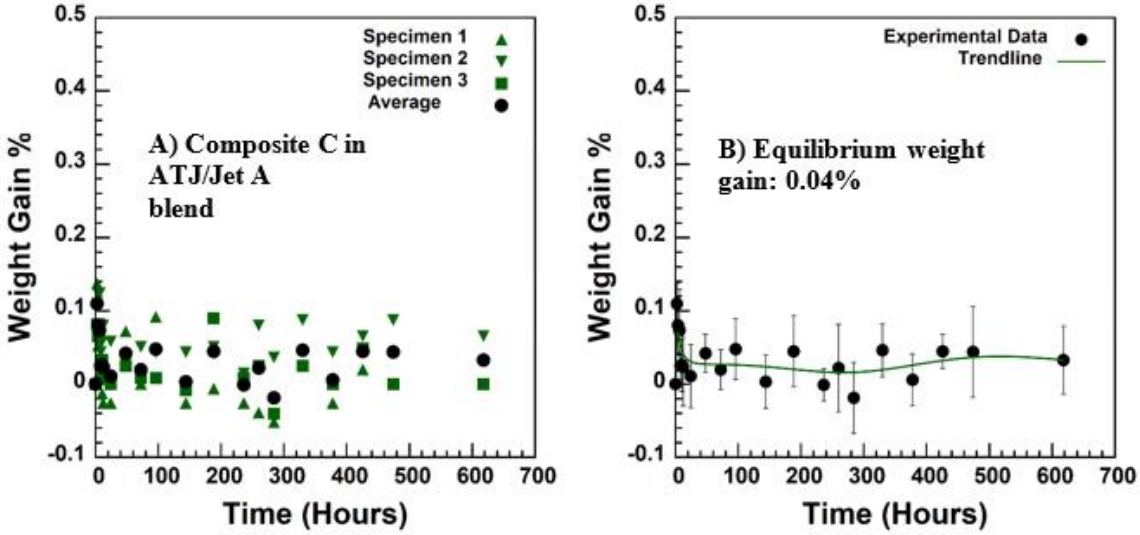

Figure 34. A) Fuel uptake by composite C of ATJ/Jet A blend and B) average weight gain versus time.

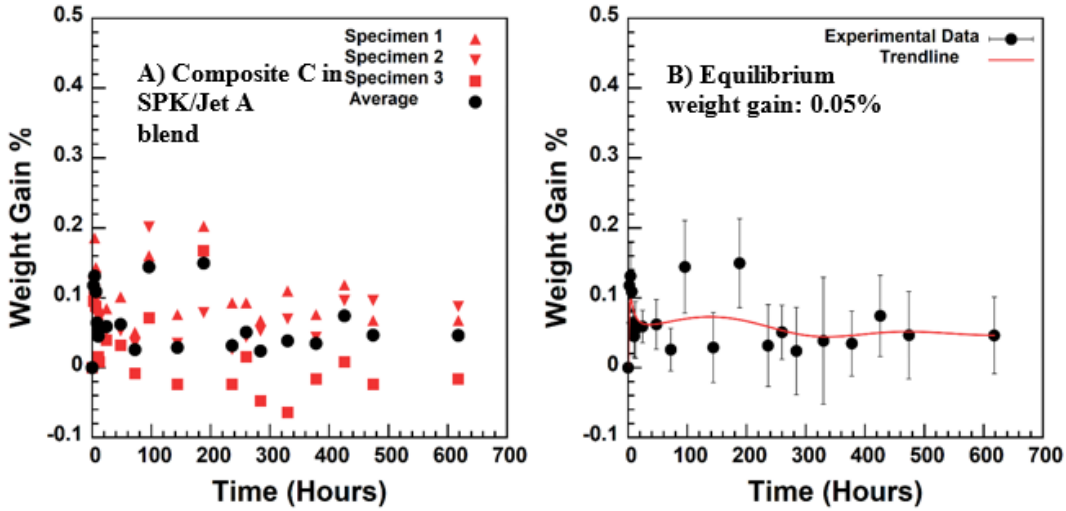

Figure 35. A) Fuel uptake by composite C of SPK/Jet A blend and B) average weight gain versus time.

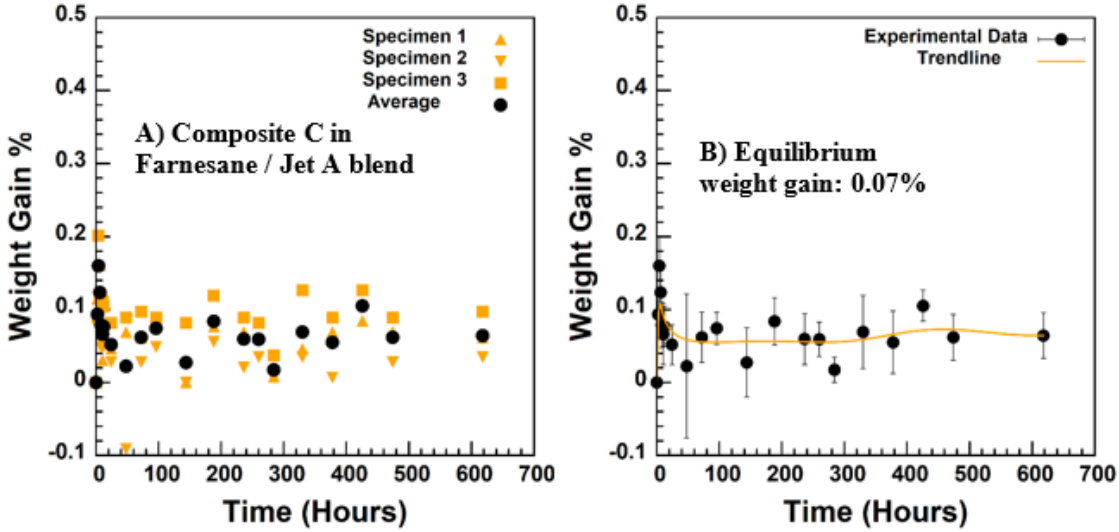

Figure 36. A) Fuel uptake by composite C of farnesane/Jet A blend and B) average weight gain versus time.

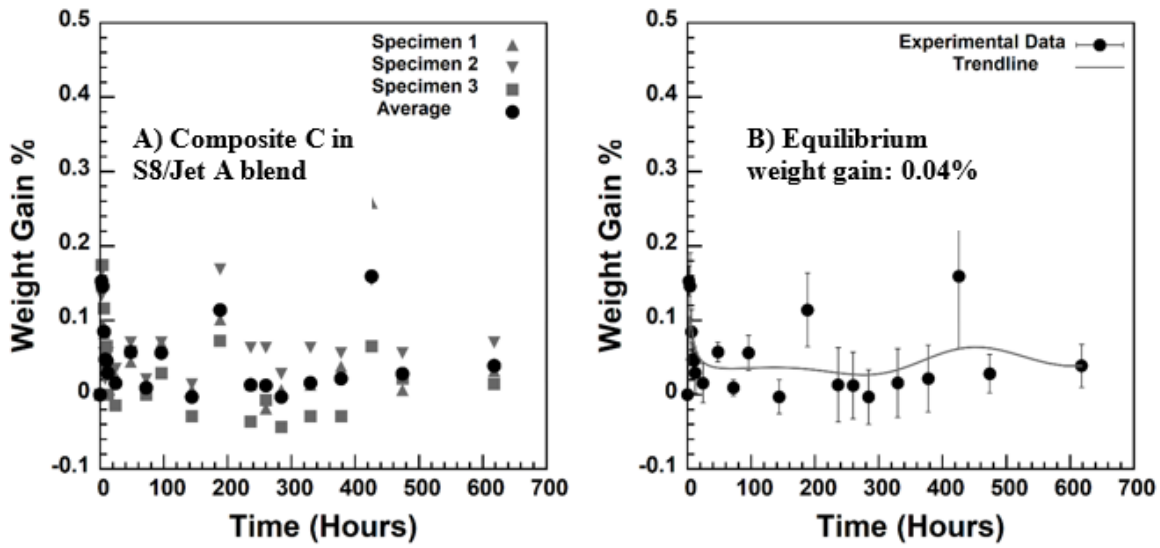

Figure 37. A) Fuel uptake by composite C of S8/Jet A blend and B) average weight gain versus time.

3.3.4 Fuel uptake for composite D

Figure 38 through Figure 42 show composite A specimens immersed separately in each of the five fuels. Please note that the solid line represents Bezier trendlines.

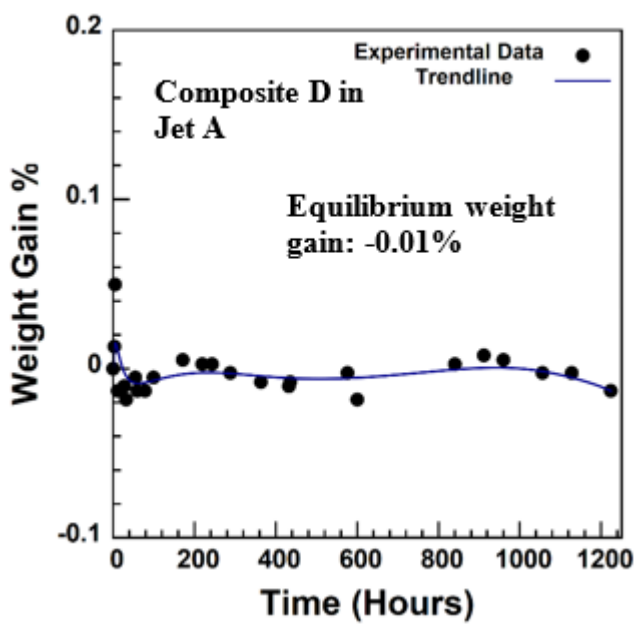

Figure 38. Jet A Fuel uptake by composite D.

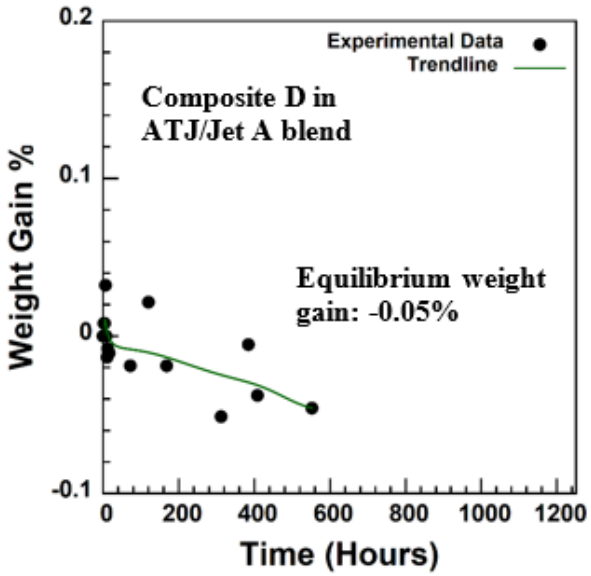

Figure 39. Fuel uptake by composite D immersed in ATJ/Jet A blend

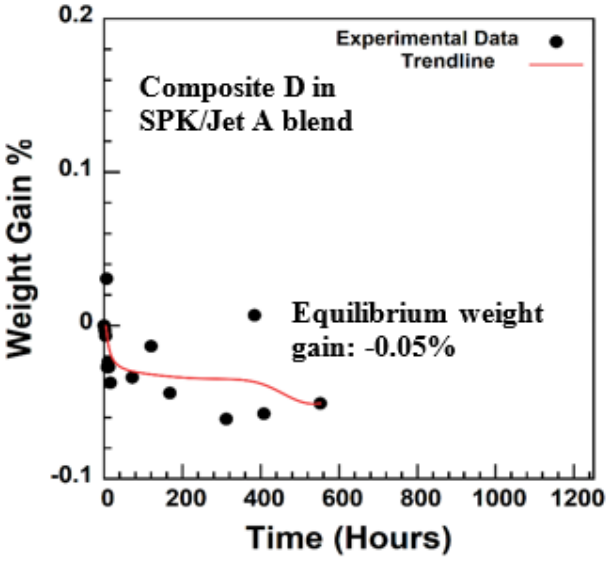

Figure 40. Fuel uptake by composite D immersed in SPK/Jet A blend.

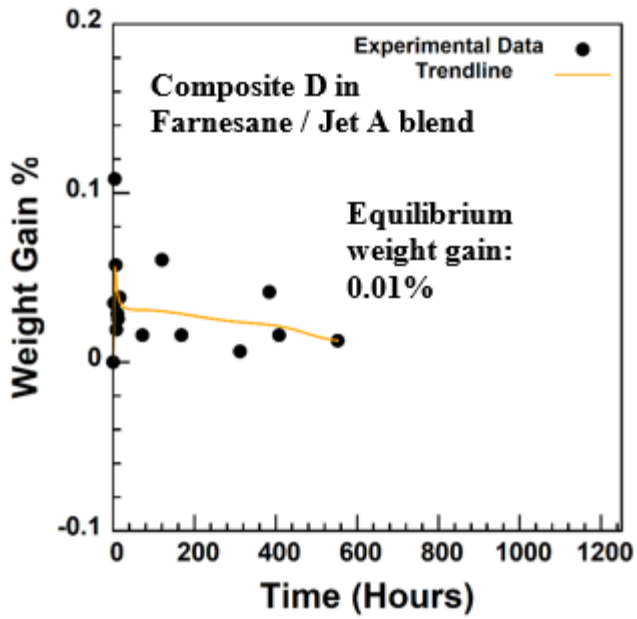

Figure 41. Fuel uptake by composite D immersed in farnesane/Jet A blend.

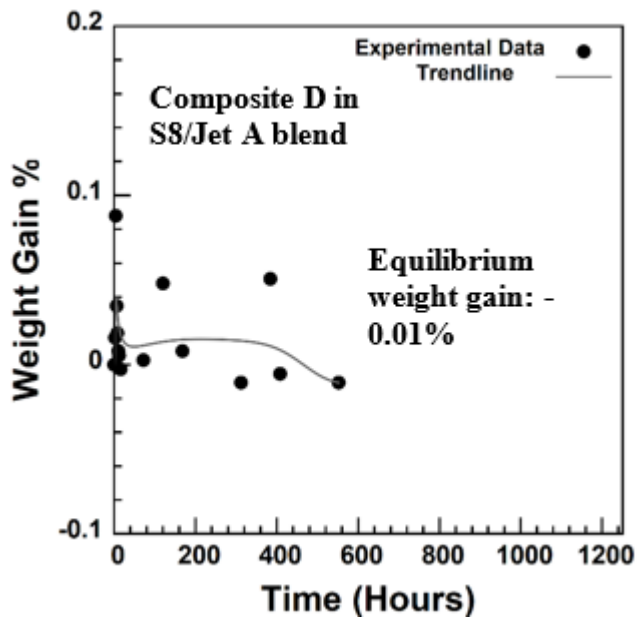

Figure 42. Fuel uptake by composite D immersed in S8/Jet A blend.

4 Dynamic mechanical analysis results for neat and fuel-exposed aerospace-grade composites

Composite materials can be exposed to different aeronautical fluids during their lifetime. These fluids can diffuse through the matrix and lead to matrix swelling, cracking, or plasticization. The fluid uptake can also degrade the fiber/matrix interface. This degradation can have a profound effect on the composites' mechanical and thermal properties, potentially leading to various failure mechanisms when subjected to mechanical loads. The interaction of the chemical components of the fluid and matrix affects diffusion. For example, the amount of fluid uptake of two different aeronautical fluids into a specific matrix can vary due to the difference in their chemical compositions. Therefore, evaluating property changes as a function of exposure to various fuels is of utmost importance to guarantee aircraft flight safety. These properties range from tensile strength, compressive strength, stiffness, etc. to glass transition temperature T_g.

In the previous section, different aerospace grade carbon/epoxy specimens were exposed to either Jet A fuel or one of four different alternative fuels blended with Jet A fuel at different weight ratios. These carbon/epoxy specimens were: *i*) Composite A: autoclave-cured Hexcel SGP370-8H/8552 eight-harness satin weave carbon/epoxy prepreg quasi-isotropic 2 x 0.5 x 0.06 in^3 with a four-ply [0/-45/+45/90] layup, *ii*) Composite B: autoclave-cured Hexcel carbon/epoxy with a four-ply $[0/90]_s$ layup, *iii*) Composite C: oven-cured Jaco Aerospace & Industrial DMS 2436 Type 1 Class 72 multi-axial warp-knit dry carbon fabric infused with API-1078 epoxy x 0.05 in^3 with a seven-ply [45/-45/0/90/0/-45/45] layup. These specimens were each individually immersed in Jet A fuel or one the four different alternative fuel blends: 50/50 Gevo ATJ /Jet A, 50/50 SPK /Jet A, 50/50 HEFA/Jet A, and 20/80 Amyris Farnesane/Jet A.

As the previous section demonstrated, the equilibrium % fuel uptake exhibited no significant differences for each set of specimens when they were immersed separately into the different fuels. DMA was performed on neat and fuel-exposed specimens to determine their T_g values. The following questions motivated the work presented in the following sections: “Will fuel uptake influence T_g?” and “How will the differences in composition between the various fuels' affect the change in T_g of the specimens immersed in these fuels?”

DMA is a technique used to measure the viscoelastic response of the material as a function of temperature and frequency. An oscillatory strain/stress is applied, as shown in Figure 43, and the material’s response in terms stress is obtained. The difference between the deformation applied and the material's response is defined as the phase angle δ.

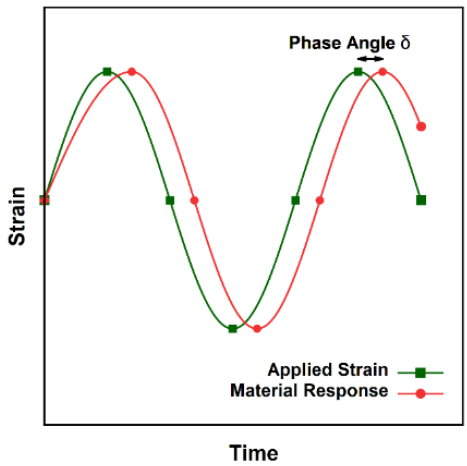

Figure 43. Oscillating stress applied to a sample and the material's response.

The strain or stress applied to the material and its stress response are represented by Figure 43 (Menard & Menard, 2002):

Applied Stress/Strain Response Stress

$$\varepsilon = \varepsilon\_0\ \sin(\omega t) or\ \sigma = \sigma\_0\ \sin(\omega t) \qquad \tau = \tau\_0\ \sin(\omega t + \delta) \tag{2}$$

Where:

ε, σ: Applied oscillatory strain/stress applied

ε_0, σ_0: Maximum applied strain/stress (or amplitude)

τ: Response stress

τ_0: Response stress amplitude

δ: Phase Angle

ω: frequency of oscillation

t: time

The viscoelasticity of a material can be understood from the phase angle δ: if δ is small, the material is highly elastic; a large δ means that the material is highly viscous (if δ=0, the material is pure elastic, if δ=90, the material is purely viscous). Mechanical properties (*e.g.*, storage modulus, loss modulus, and tan(delta)) are determined from the material's response. The modulus of a material indicates its resistance to deformation. E' is the elastic (storage) modulus, which measures the elasticity of the material and its ability to store energy. E'' is the viscous

(loss) modulus, which evaluates the capability of a material to dissipate energy. E' and E'' are obtained through Equation 3:

$$E\hat{}' = \tau\_0/\varepsilon\_0 \ \ \cos(\delta) \ \ and \ E'' = \ \ [\![\tau\_0/\varepsilon\_0 \ \ \sin]\!] \ (\delta) \tag{3}$$

The tangent (δ) represents the ratio of the E'' with respect to E'; it is also defined as the damping of the material ($tan(\delta)=E''/E'$). Figure 44 represents an example of DMA results of composite B specimen immersed in ATJ/Jet A fuel blend. The logarithm of E', E'', and $tan\ \delta$ curves as a function of the temperature are plotted.

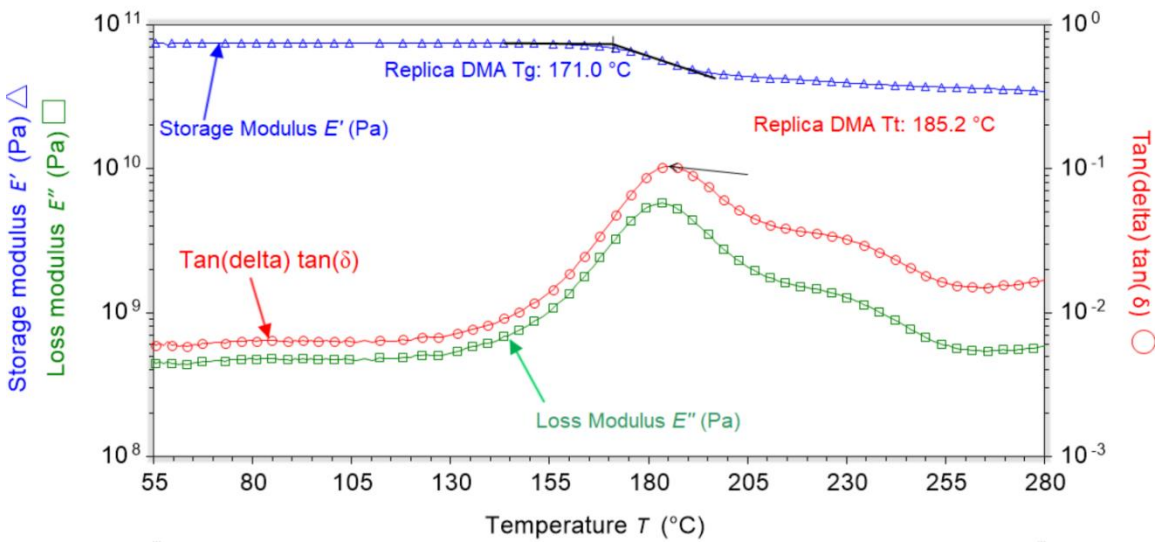

Figure 44. Sample dynamic mechanical analysis results.

As the temperature increases, amorphous thermoset materials (*e.g.*, epoxy) will undergo several transitions, as shown in Figure 45.

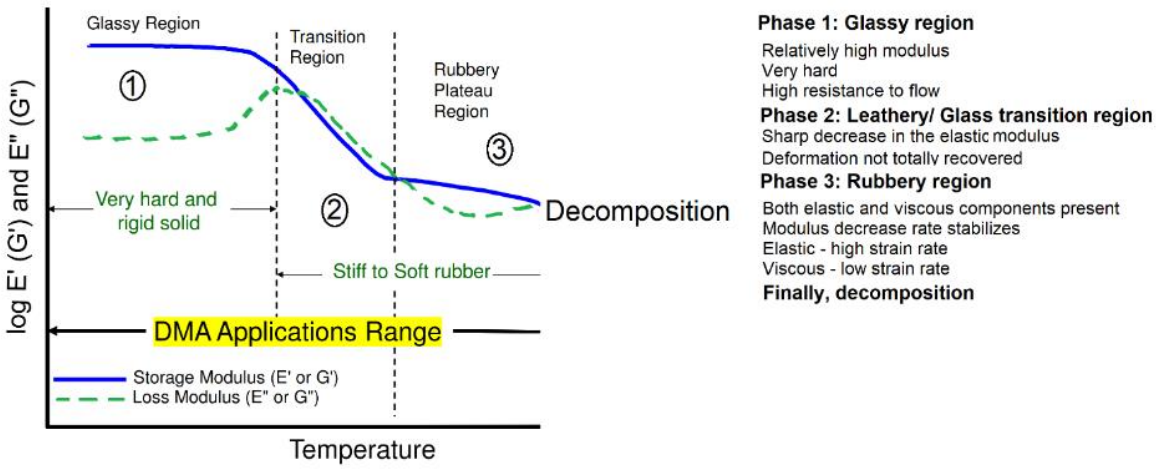

Figure 45. Regions of viscoelastic behavior for a thermoset polymer.

At low temperatures, amorphous polymers are in the glassy (sometimes referred to as *vitreous*) state where they are stiff. Upon heating, these epoxy polymers undergo increased molecular motion. This occurs at a temperature range known as the glass-rubber transition region. This temperature range is critical since the composite's properties can differ drastically as the temperature traverses and rises above the T_g range. As measured in DMA, E' decreases during glass transition. This decrease comes with a peak in E'' leading to a peak in $\tan\delta$. The ASTM 7028-07: Standard Test Method for Glass Transition Temperature (DMA T_g) of Polymer Matrix Composites by Dynamic Mechanical Analysis (DMA) (ASTM International, 2016) defines two temperatures that indicate this transition. The intersection point of the two tangent lines of E' during the glass transition is defined as DMA T_g, while the temperature at which $\tan\delta$ curve peaks is defined as DMA T_t. Fuel diffusion into carbon/epoxy specimens leads to swelling of the epoxy, which causes enhanced molecular mobility of the crosslinked chains between the crosslinks. This segmental motion may, in turn, lower the glass transition temperature.

DMA is important for this work since it allows one to investigate the effects of fuel absorption on T_g. The change in T_g can indicate a change in other mechanical properties. The analysis presented in this report was performed following the ASTM 7028-07 (ASTM International, 2016). The DMA parameters used for all specimens in agreement with the standard are listed in Table 11.

Table 11. Dynamic Mechanical Analysis parameters used in the study

Test Method	**Preconditioning**	**Heating Rate**	**Frequency**
Three-point bending	Vacuum at an absolute pressure of 15 inHg (0.5 atm) at room temperature + controlled humidity chamber (50% RH)	5 °C/min	1 Hz

DMA was performed on neat and fuel-immersed specimens using an RSA-G2 Solids Analyzer (shown in Figure 46) using the three-point bending mode. In this mode, the specimen is supported at two ends, a strain is applied at the middle. It is the preferred mode for testing solid specimens of stiff materials such as composites.

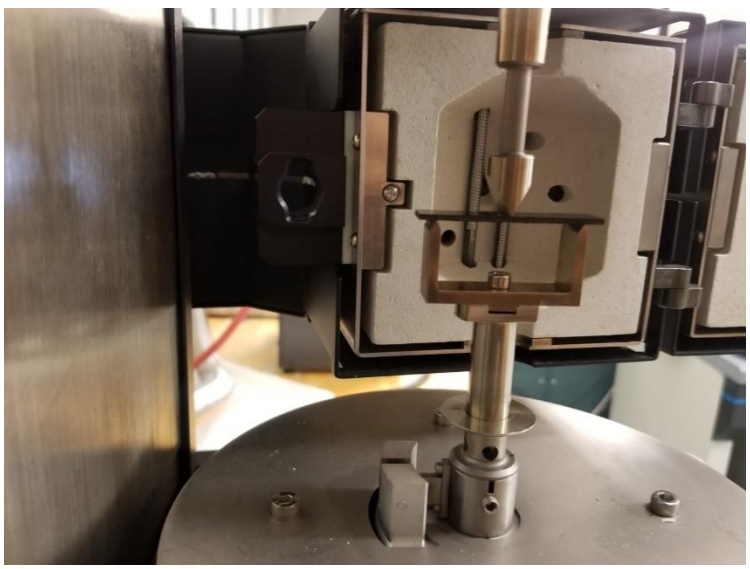

Figure 46. Three-point bending mode and RSA-G2 solids analyzer.

Specimens were first preconditioned at an absolute pressure of 15 inHg (0.5 atm) at room temperature, after which specimens were kept in a controlled humidity chamber at 50% RH. This step was done to ensure similar testing conditions for all specimens since different initial moisture content can affect the T_g values. The exposed specimens were then immersed in different fuels until saturation. The neat and fuel-exposed specimens were tested within 30 minutes after being removed from either the controlled humidity chamber or from the fuels, as suggested by the ASTM standard (ASTM International, 2016).

A 5°C/min heating rate was used for all specimens included in the DMA results since changing the heating rate may affect the T_g . This heating rate represents a good compromise between

measurement precision and test method convenience for wet composites, given that a lower heating rate will cause soak fuel to evaporate from the specimens.

Although an absolute size is not predetermined by the standard, it a span-to-thickness ratio greater than ten is recommended. To comply with that recommendation, three 2 x 0.5 in^2 replicas for each type of composite were used. Each set of specimens had a different thickness, but overall specimen dimensions respected the span-to-thickness ratio imposed by the standard (Figure 47). The span-to-thickness ratio for composites A-B and C are 33 and 40, respectively.

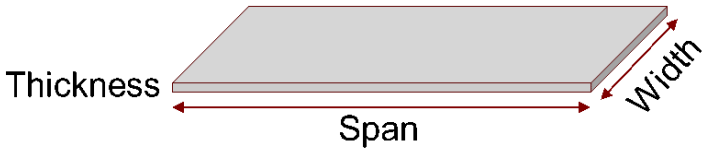

Figure 47. Specimen dimensions.

Representative DMA results are shown in Figure 48 for a set of three carbon/epoxy replicas (composite A). The storage modulus for the three replicas displayed no distinctive differences in DMA T_g and DMA T_t values.

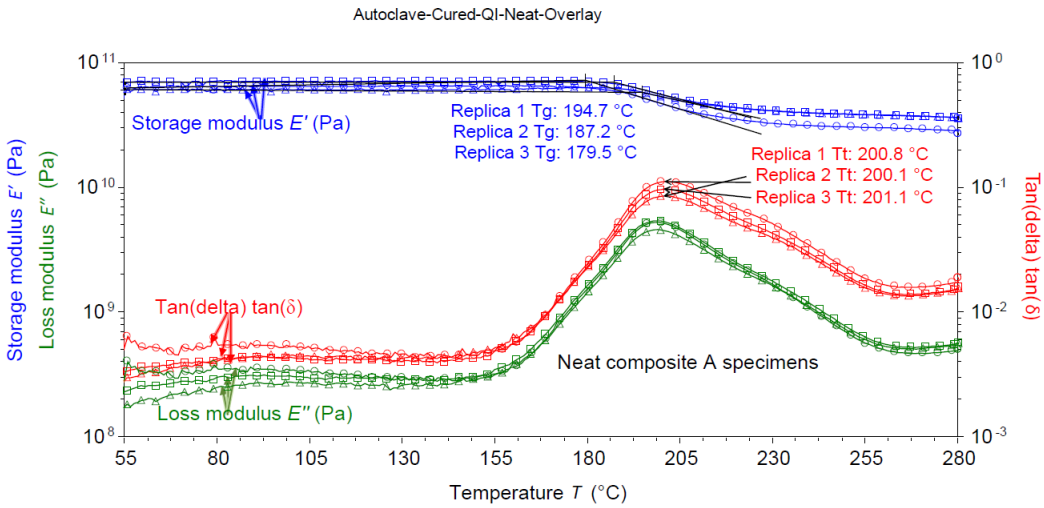

Figure 48. Dynamic Mechanical Analysis results for neat composite A specimens.

Table 12 summarizes DMA results obtained for neat and fuel-exposed specimens used in the study.

Table 12. Dynamic Mechanic Analysis results summary

Specimen type	**Property**	**Neat / Exposed**		**Exposed to Jet A**	**Exposed to ATJ/Jet A blend**	**Exposed to SPK/Jet A blend**	**Exposed to Farnesane /Jet A blend**	**Exposed to S8/Jet A**
A	DMA T_g (°C)	Neat	Average ± Standard Deviation	187.1 ± 7.6	187.1 ± 7.6	187.1 ± 7.6	187.1 ± 7.6	187.1 ± 7.6
			Range (low-high)	179.5 – 194.7	179.5 – 194.7	179.5 – 194.7	179.5 – 194.7	179.5 – 194.7
		Fuel-Exposed	Average ± Standard Deviation	174 ± 1.5	173.5 ± 0.8	173.3 ± 0.9	172.9 ± 0.9	173.5 ± 0.1
			Range (low-high)	172.3-175.3	172.9 – 174.5	172.3 – 174.2	172.3 – 173.9	173.4 – 173.7
	Tangent delta (δ) peak T_t (°C)	Neat	Average ± Standard Deviation	200.6 ± 0.5	200.6 ± 0.5	200.6 ± 0.5	200.6 ± 0.5	200.6 ± 0.5
			Range (low-high)	200.1 – 201.1	200.1 – 201.1	200.1 – 201.1	200.1 – 201.1	200.1 – 201.1
		Fuel-Exposed	Average ± Standard Deviation	186.9 ± 0.8	187.9 ± 0.7	188.0 ± 0.15	186.7 ± 1.3	187.4 ± 0.9
			Range (low-high)	186 – 187.5	187.2 – 188.6	187.9 – 188.2	185.3 – 187.9	186.5 – 188.3
B	DMA T_g (°C)	Neat	Average ± Standard Deviation	182.3 ± 0.26	182.3 ± 0.26	182.3 ± 0.26	182.3 ± 0.26	182.3 ± 0.26
			Range (low-high)	182.1-182.6	182.1-182.6	182.1-182.6	182.1-182.6	182.1-182.6
		Fuel-Exposed	Average ± Standard Deviation	168.9 ± 0.4	170.1 ± 1.3	171.4 ± 0.3	172.3 ± 0.7	170.6 ± 0.9
			Range (low-high)	168.5 – 169.3	168.6-170.9	171.1 – 171.7	171.5 – 172.9	169.6 – 171.2
	Tangent delta (δ) peak T_t (°C)	Neat	Average ± Standard Deviation	198.9 ± 0	198.9 ± 0	198.9 ± 0	198.9 ± 0	198.9 ± 0
			Range (low-high)	198.9-198.9	198.9-198.9	198.9-198.9	198.9-198.9	198.9-198.9
		Fuel-Exposed	Average ± Standard Deviation	185.5 ± 2.1	184.5 ± 1.0	185.4 ± 0.9	185.8 ± 0.34	183.4 ± 1.1
			Range (low-high)	183.4 – 187.6	183.4 - 185.2	184.4 - 186.3	185.6 - 186.2	182.6 - 184.6

Specimen type	Property	Neat / Exposed		Exposed to Jet A	Exposed to ATJ/Jet A blend	Exposed to SPK/Jet A blend	Exposed to Farnesane /Jet A blend	Exposed to S8/Jet A
C	DMA T_g (°C)	Neat	Average ± Standard Deviation	168.4 ± 0.5	168.4 ± 0.5	168.4 ± 0.5	168.4 ± 0.5	168.4 ± 0.5
			Range (low-high)	168.1 - 168.8	168.1 - 168.8	168.1 - 168.8	168.1 - 168.8	168.1 - 168.8
		Fuel-Exposed	Average ± Standard Deviation	165.3 ± 0	167.3 ± 0.2	168.2 ± 0.3	166.3 ± 0.1	165.7 ± 0.6
			Range (low-high)	165.3 – 165.3	167.2 – 167.5	168 – 168.5	166.3 – 166.4	165.3 – 166.2
	Tangent delta (δ) peak T_t (°C)	Neat	Average ± Standard Deviation	182.9 ± 0.1	182.9 ± 0.1	182.9 ± 0.1	182.9 ± 0.1	182.9 ± 0.1
			Range (low-high)	182.8 - 183	182.8 - 183	182.8 - 183	182.8 - 183	182.8 - 183
		Fuel-Exposed	Average ± Standard Deviation	182.55 ± 1.8	183.4 ± 0.4	182.5 ± 0.5	183.1 ± 0.1	181.2 ± 0.1
			Range (low-high)	181.3-183.8	183.1 – 183.7	182.1 – 182.9	183 – 183.2	181.2 – 181.3

In this table, the first row for each neat and fuel-exposed specimen represents the average T_g and DMA T_t values and the standard deviation from three replicates, whereas the second row contains the DMA T_g and DMA T_t range for three neat and fuel-exposed replicates. The tables shows that the DMA T_g and T_t of specimens immersed in all types of fuels decreased by the same degree. DMA T_g decreased by an average of 14.6°C, 19.0°C, and 3.1°C, for composites A, B and C, respectively. Also, DMA T_t decreased by 20.6°C for Hexcel [0/- 45/45/90], by 18.0°C for Hexcel $[0/90]_s$, and 1.8°C for DMS2436/API-1078 carbon/epoxy specimens.

The following key conclusions can be drawn based on the results summarized in Table 12:

- The T_g and T_t decrease of fuel-exposed composites A and B was more significant than that of fuel-exposed composite C, meaning that the difference in T_g and T_t between neat and fuel-exposed specimens was greater in composites A and B than in composite C.
- DMA T_g and DMA T_t for specimens saturated with the four alternative fuel blends were not differently impacted than those saturated with Jet A fuel. Therefore, a higher weight fraction of alternative fuels in the four blends could potentially be permitted.

- There was a direct correlation between fuel uptake results and DMA results of fuel-exposed composites. DMA T_g and DMA T_t of the different composites immersed in different fuels that had similar fuel uptake decreased within the same range.
- Alternative fuels blended with Jet A fuel up to the different ratios studied herein, can replace the use of conventional jet fuels, based on their effect on DMA T_g and DMA T_t of the different aerospace carbon/epoxy composites, which is in the same range to that of Jet A fuel.

4.1 Dynamic mechanical analysis results for all specimens

4.1.1 Dynamic mechanical analysis results for composite A

Figure 49 through Figure 54 show the DMA results for neat and fuel-exposed composite A specimens. Table 13 summarizes these results.

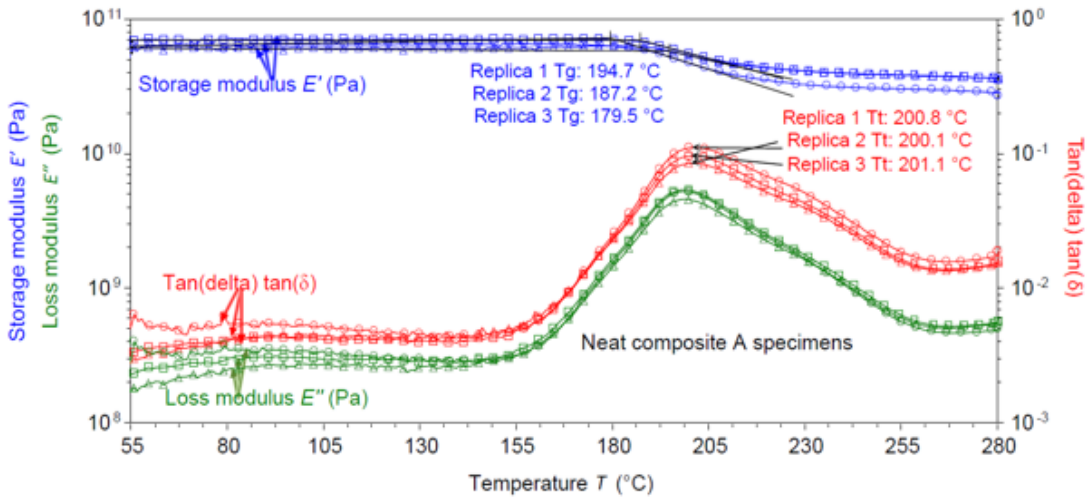

Figure 49. DMA results for three neat composite A specimens.

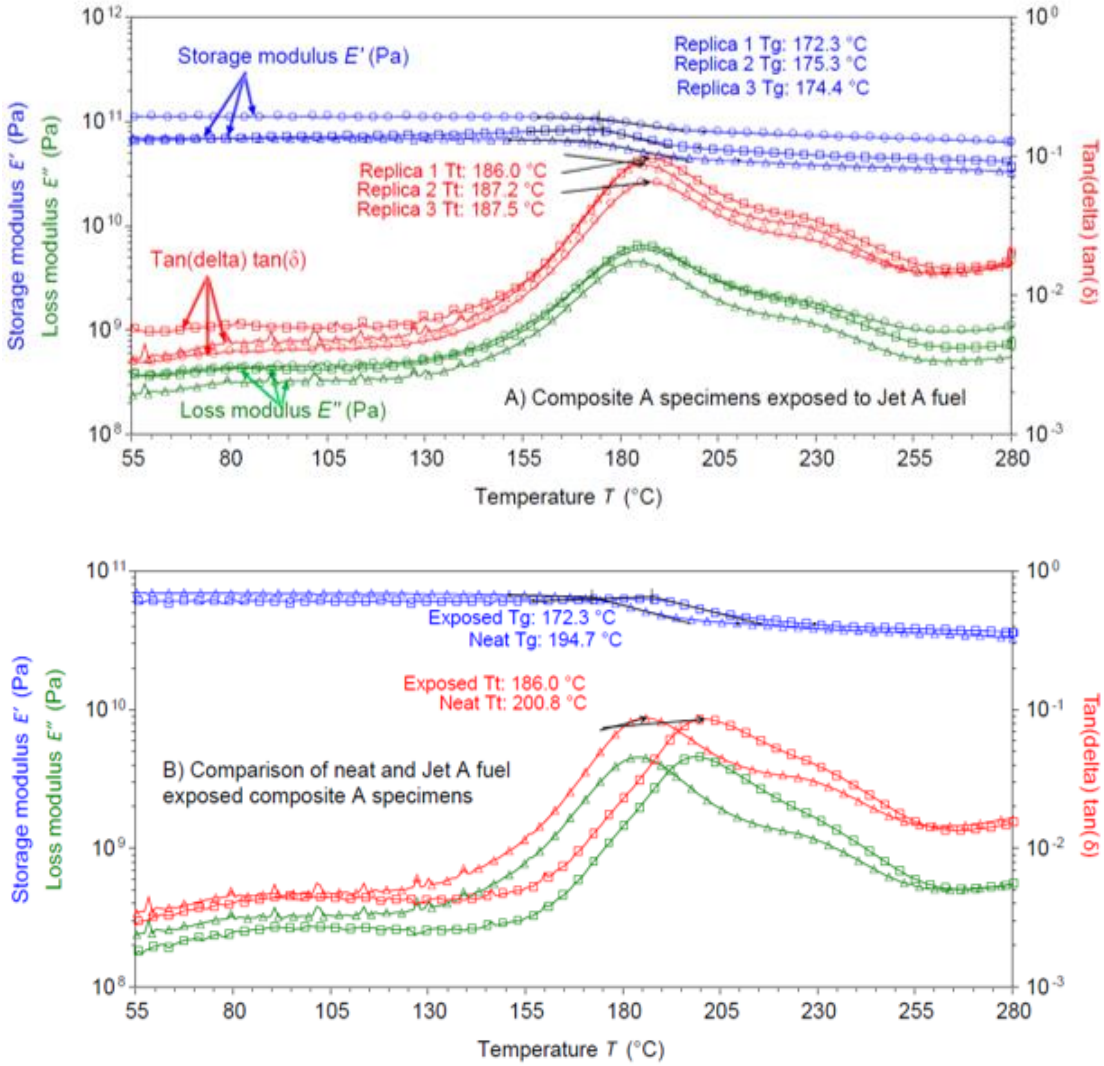

Figure 50. A) DMA results of composite A specimens immersed in Jet A fuel for 700 hours. (B) Comparison of one neat and one fuel exposed composite A specimen.

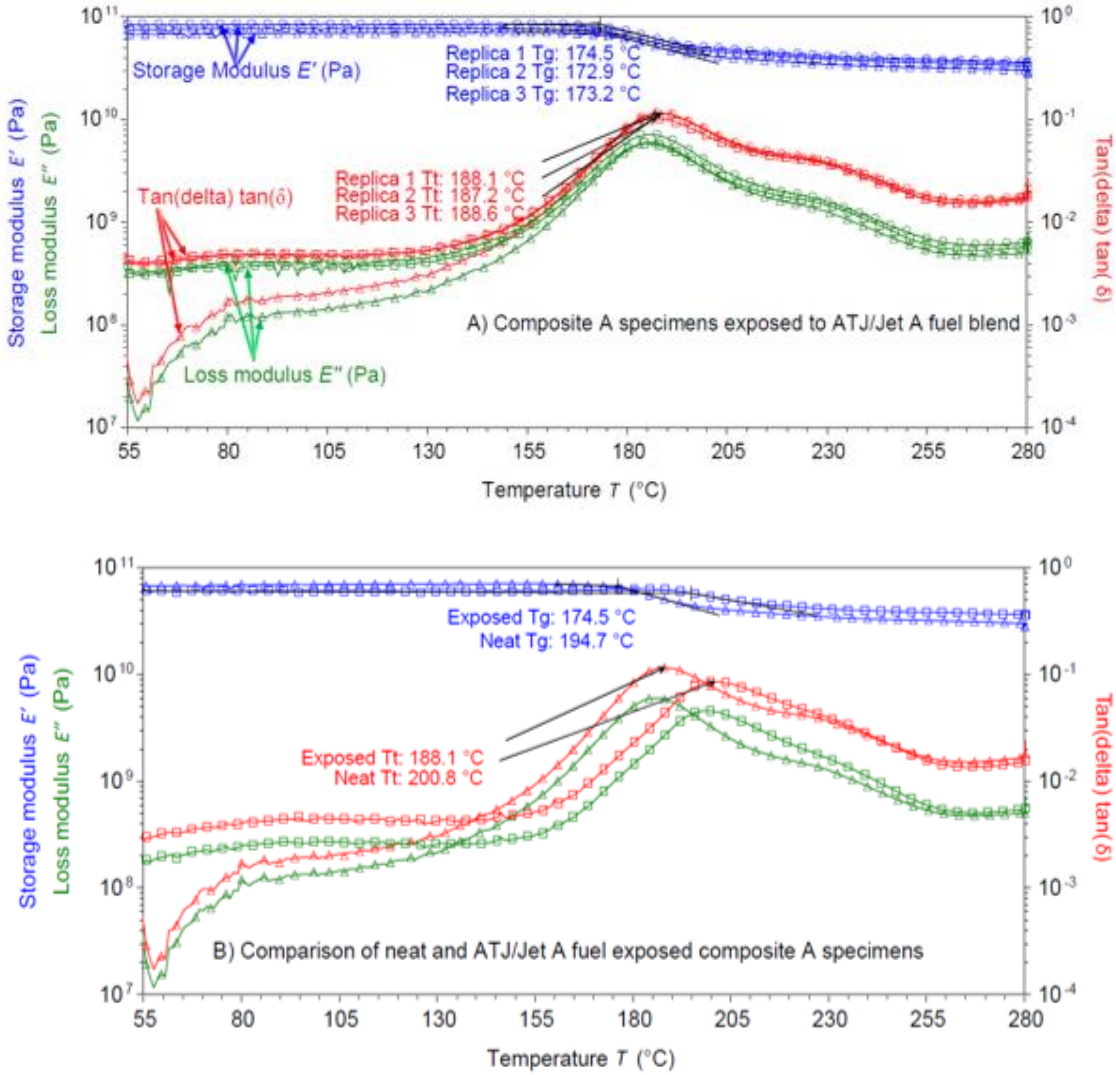

Figure 51. A) DMA results of composite A specimens immersed in ATJ/Jet A blend for 700 hours. (B) Comparison of one neat and one exposed composite A specimen.

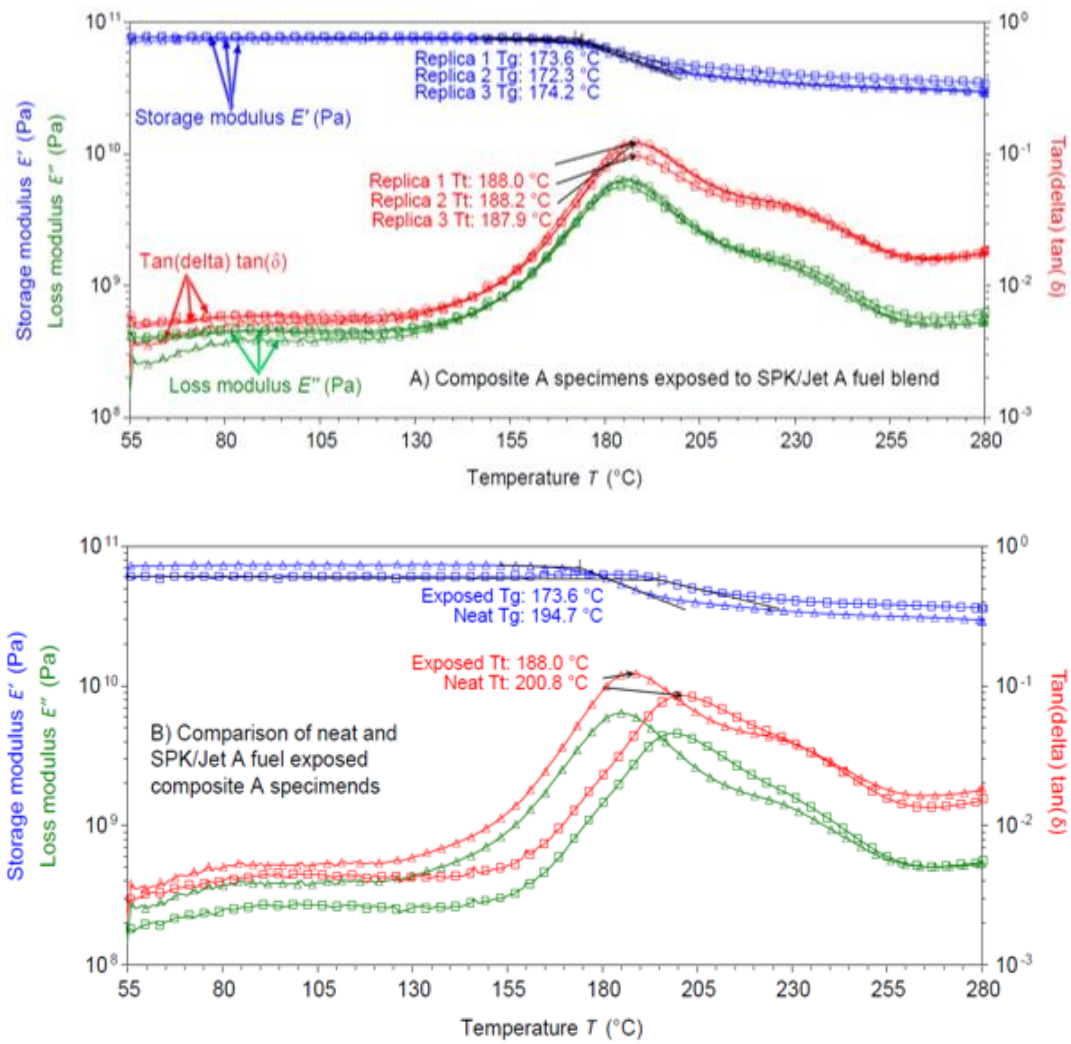

Figure 52. A) DMA results of composite A specimens immersed in SPK/Jet A blend for 700 hours. (B) Comparison of one neat and one exposed composite A specimen.

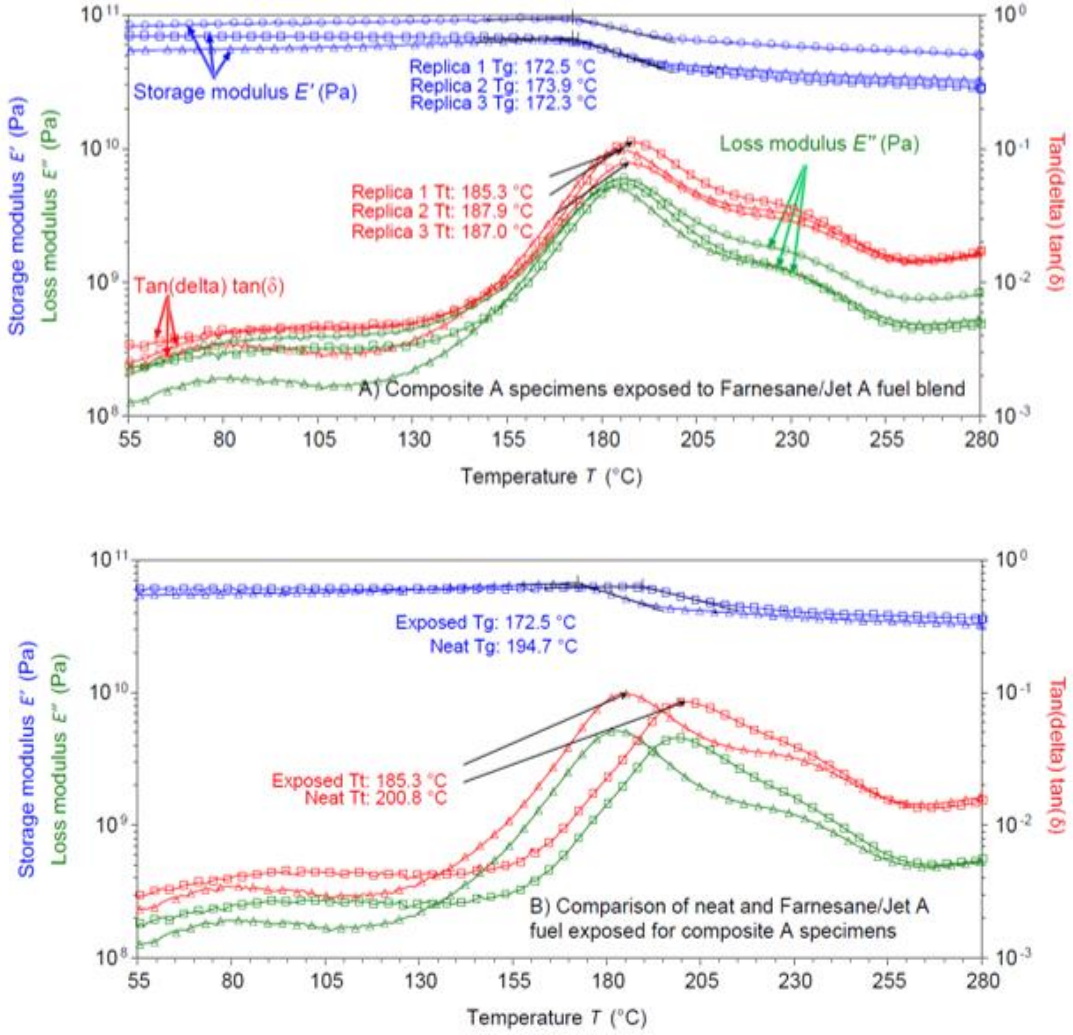

Figure 53. A) DMA results of composite A specimens immersed in Farnesane/Jet A blend for 700 hours. (B) Comparison of one neat and one exposed composite A specimen.

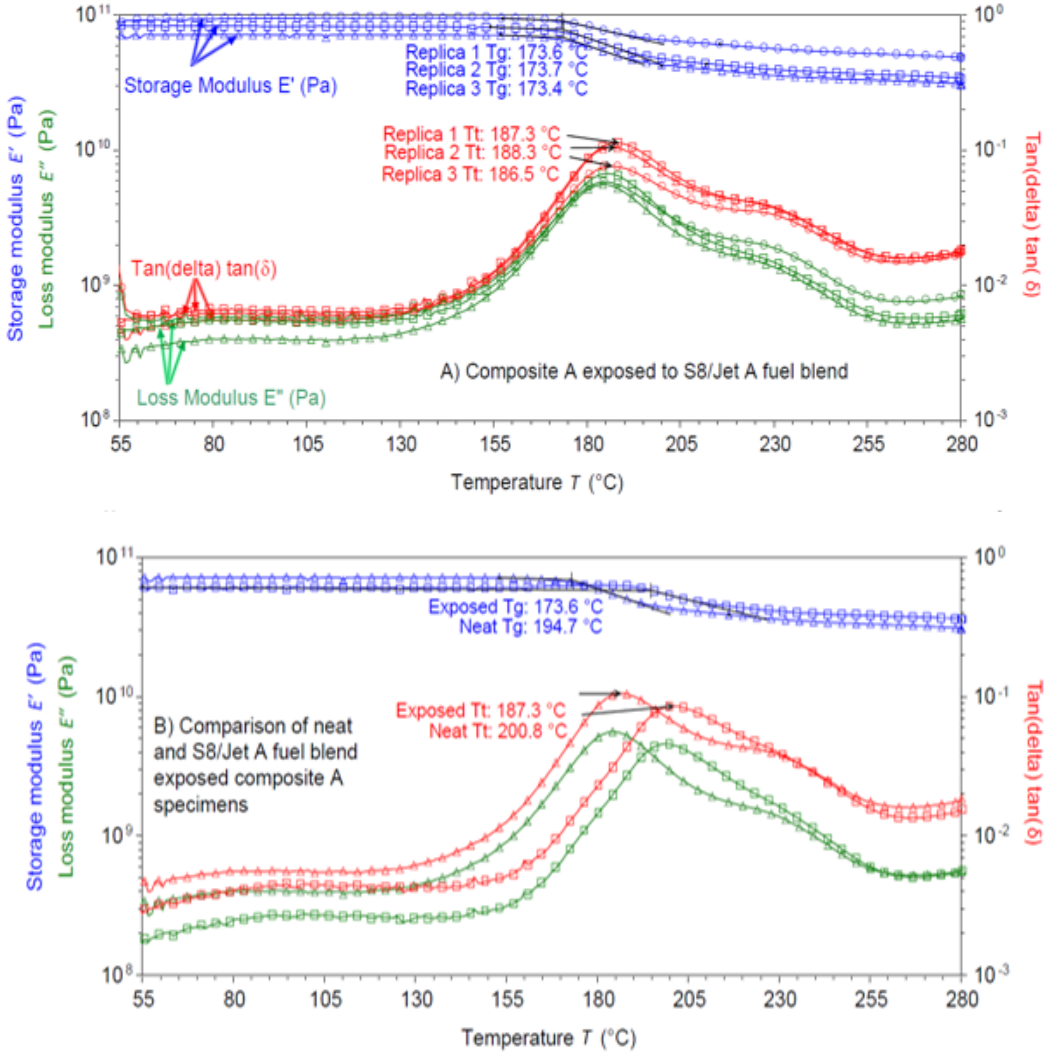

Figure 54. A) DMA results of composite A specimens immersed in S8/Jet A blend for 700 hours. (B) Comparison of one neat and one exposed composite A specimen.

Table 13. Dynamic Mechanical Analysis results for composite A specimens

Specimen type	**Property**	**Neat / Exposed**		**Exposed to Jet A**	**Exposed to ATJ/Jet A blend**	**Exposed to SPK/Jet A blend**	**Exposed to Farnesane /Jet A blend**	**Exposed to S8/Jet A**
A	**DMA T_g (°C)**	**Neat**	**Average ± Standard Deviation**	187.1 ± 7.6	187.1 ± 7.6	187.1 ± 7.6	187.1 ± 7.6	187.1 ± 7.6
			Range (low-high)	179.5 – 194.7	179.5 – 194.7	179.5 – 194.7	179.5 – 194.7	179.5 – 194.7
		Fuel-Exposed	**Average ± Standard Deviation**	174 ± 1.5	173.5 ± 0.8	173.3 ± 0.9	172.9 ± 0.9	173.5 ± 0.1
			Range (low-high)	172.3-175.3	172.9 – 174.5	172.3 – 174.2	172.3 – 173.9	173.4 – 173.7
	Tangent delta (δ) peak T_t (°C)	**Neat**	**Average ± Standard Deviation**	200.6 ± 0.5	200.6 ± 0.5	200.6 ± 0.5	200.6 ± 0.5	200.6 ± 0.5
			Range (low-high)	200.1 – 201.1	200.1 – 201.1	200.1 – 201.1	200.1 – 201.1	200.1 – 201.1
		Fuel-Exposed	**Average ± Standard Deviation**	186.9 ± 0.8	187.9 ± 0.7	188.0 ± 0.15	186.7 ± 1.3	187.4 ± 0.9
			Range (low-high)	186 – 187.5	187.2 – 188.6	187.9 – 188.2	185.3 – 187.9	186.5 – 188.3

4.1.2 Dynamic mechanical analysis results for composite B

Figure 55 through Figure 60 show the DMA results for neat and fuel-exposed composite B specimens. Table 14 summarizes these results.

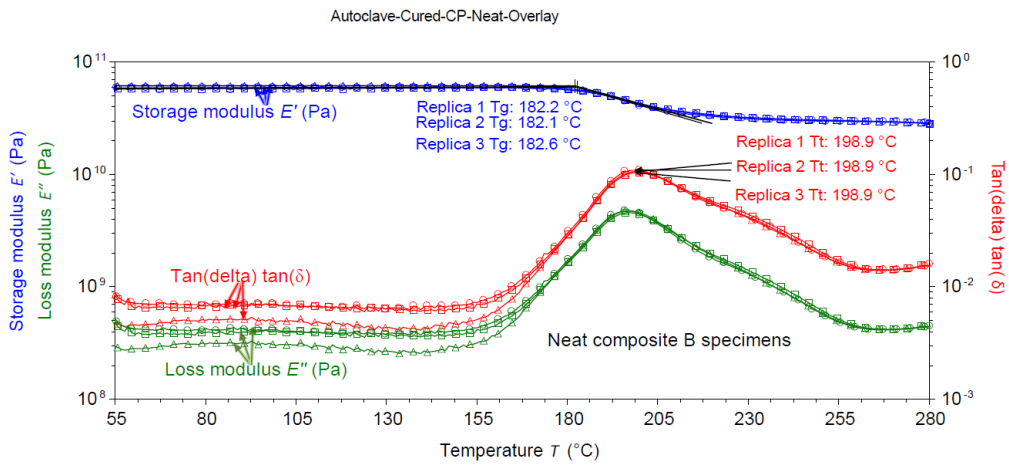

Figure 55. DMA results for three neat composite B specimens.

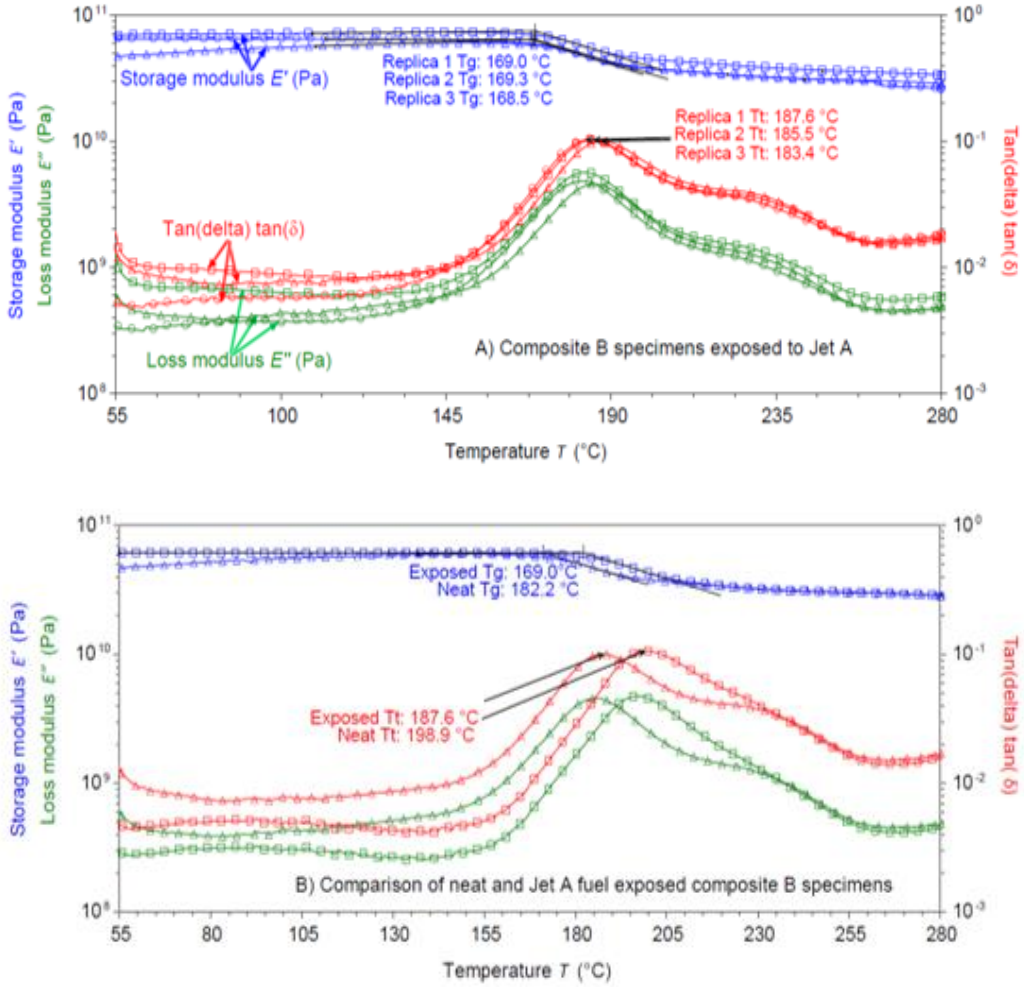

Figure 56. A) DMA results of composite B specimens immersed in Jet A for 700 hours. (B) Comparison of one neat and one exposed composite B specimen.

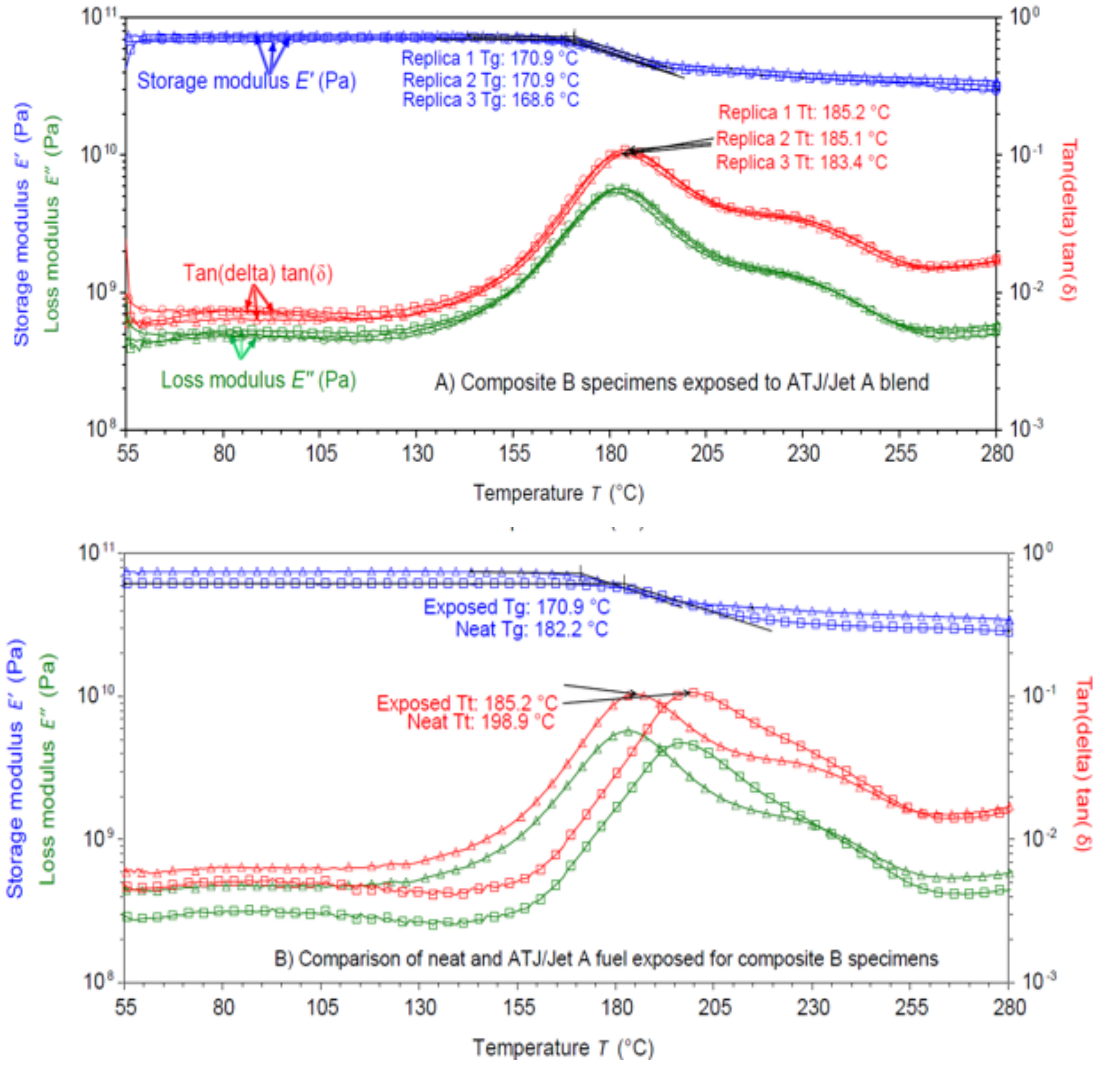

Figure 57. A) Dynamic Mechanical Analysis results of composite B specimens immersed in ATJ/Jet A blend for 700 hours and B) a comparison of one neat and one fuel-exposed composite B specimen.

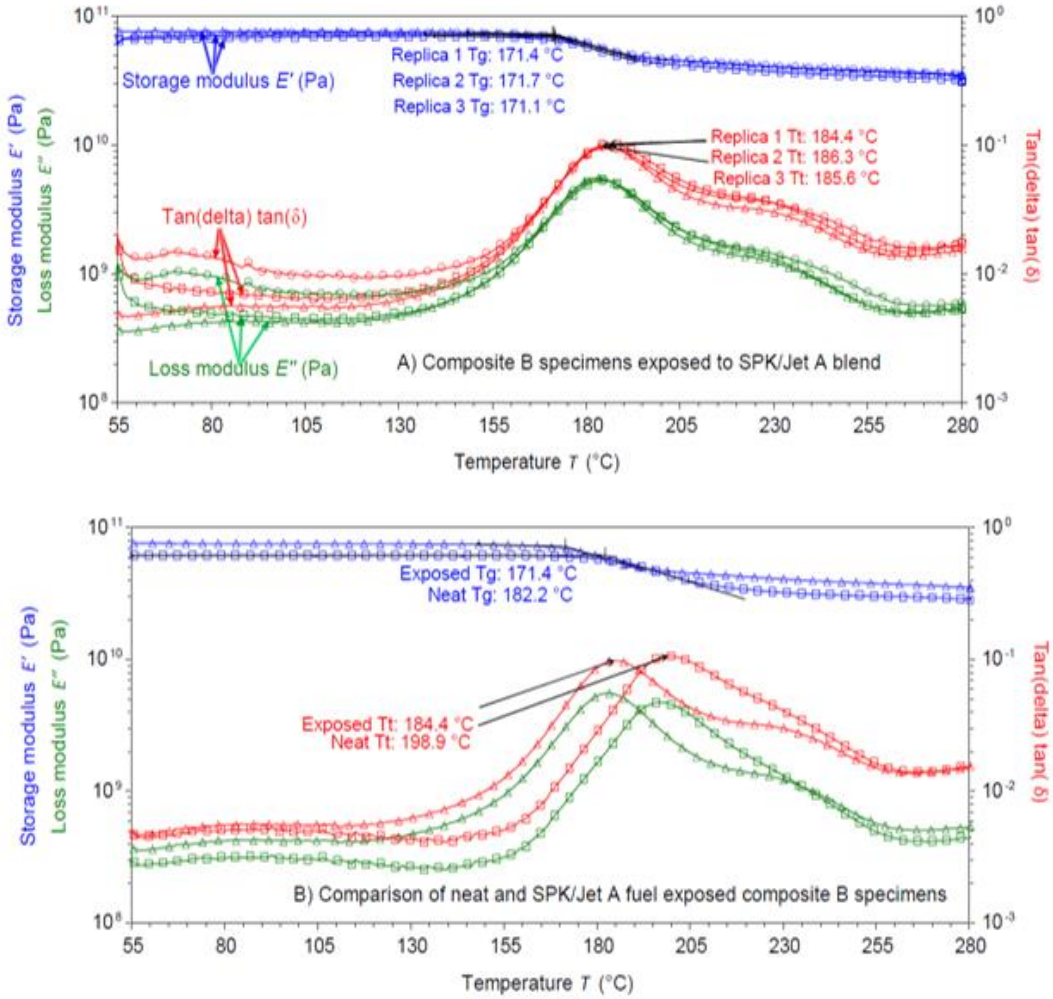

Figure 58. A) DMA results of composite B specimens immersed in SPK/Jet A blend for 700 hours and B) a comparison of one neat and one fuel-exposed composite B specimen.

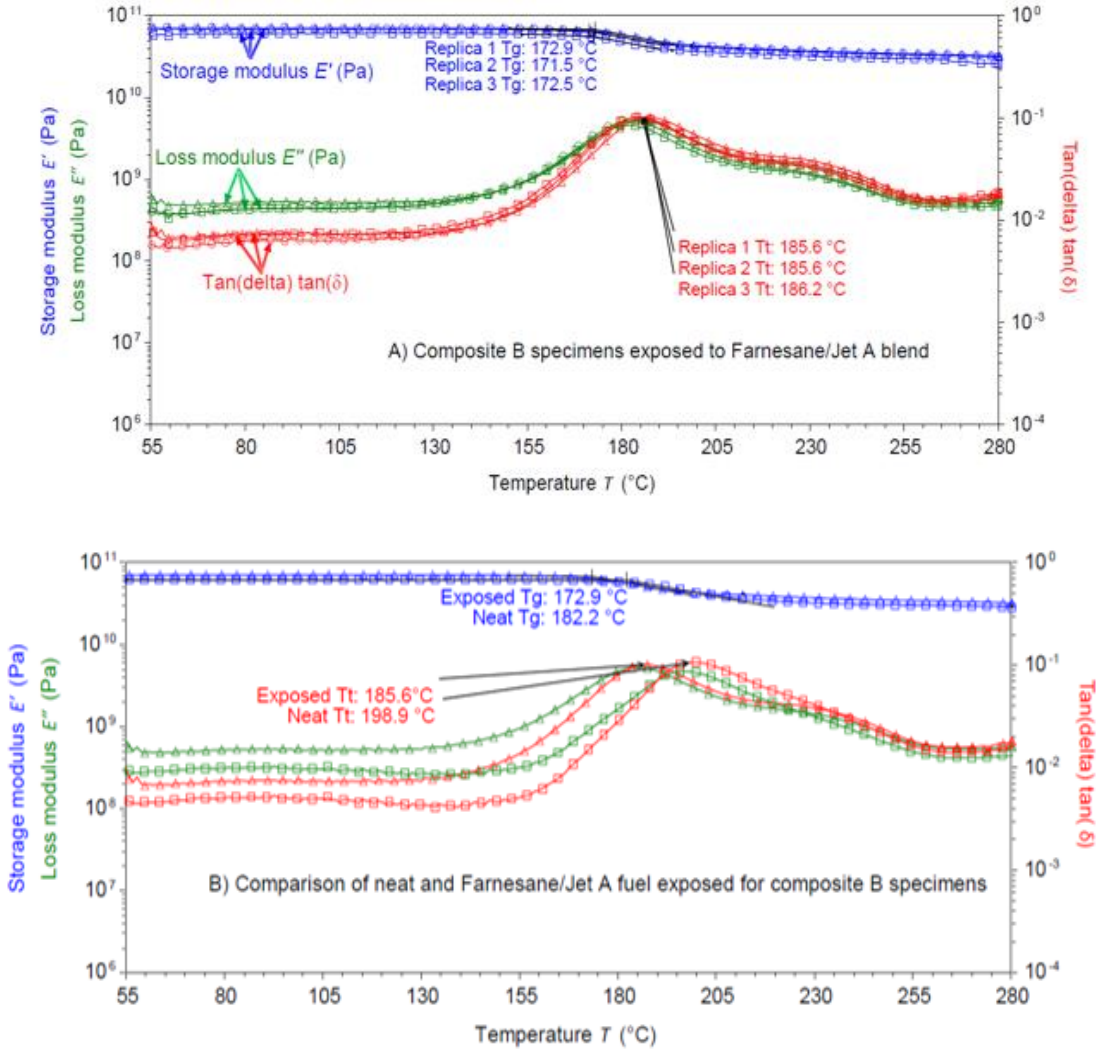

Figure 59. A) DMA results of composite B specimens immersed in Farnesane/Jet A blend for 700 hours and B) a comparison of one neat and one fuel-exposed composite B specimen.

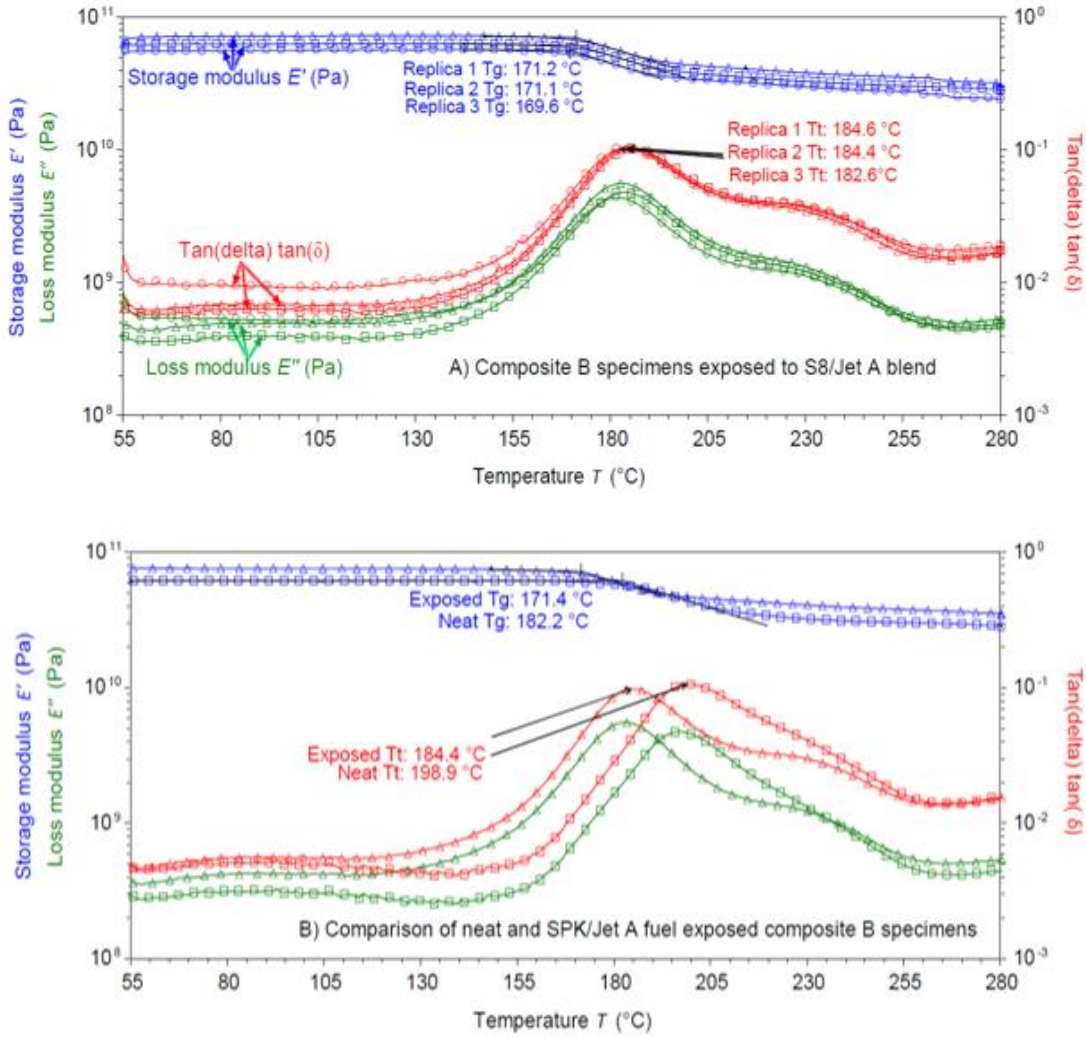

Figure 60. A) DMA results of composite B specimens immersed in S8/Jet A blend for 700 hours and B) a comparison of one neat and one fuel-exposed composite B specimen.

Table 14. DMA results for composite B specimens.

Specimen type	Property	Neat / Exposed		Exposed to Jet A	Exposed to ATJ/Jet A blend	Exposed to SPK/Jet A blend	Exposed to Farnesane /Jet A blend	Exposed to S8/Jet A
B	**DMA Tg (°C)**	**Neat**	**Average ± Standard Deviation**	182.3 ± 0.26	182.3 ± 0.26	182.3 ± 0.26	182.3 ± 0.26	182.3 ± 0.26
			Range (low-high)	182.1-182.6	182.1-182.6	182.1-182.6	182.1-182.6	182.1-182.6
		Fuel-Exposed	**Average ± Standard Deviation**	168.9 ± 0.4	170.1 ± 1.3	171.4 ± 0.3	172.3 ± 0.7	170.6 ± 0.9
			Range (low-high)	168.5 – 169.3	168.6-170.9	171.1 – 171.7	171.5 – 172.9	169.6 – 171.2
	Tangent delta (δ) peak T_t (°C)	**Neat**	**Average ± Standard Deviation**	198.9 ± 0	198.9 ± 0	198.9 ± 0	198.9 ± 0	198.9 ± 0
			Range (low-high)	198.9-198.9	198.9-198.9	198.9-198.9	198.9-198.9	198.9-198.9
		Fuel-Exposed	**Average ± Standard Deviation**	185.5 ± 2.1	184.5 ± 1.0	185.4 ± 0.9	185.8 ± 0.34	183.4 ± 1.1
			Range (low-high)	183.4 – 187.6	183.4 - 185.2	184.4 - 186.3	185.6 - 186.2	182.6 - 184.6

4.1.3 Dynamic mechanical analysis results for composite C

Figure 61 through Figure 66 show the DMA results for composite C. Table 15 summarizes these results.

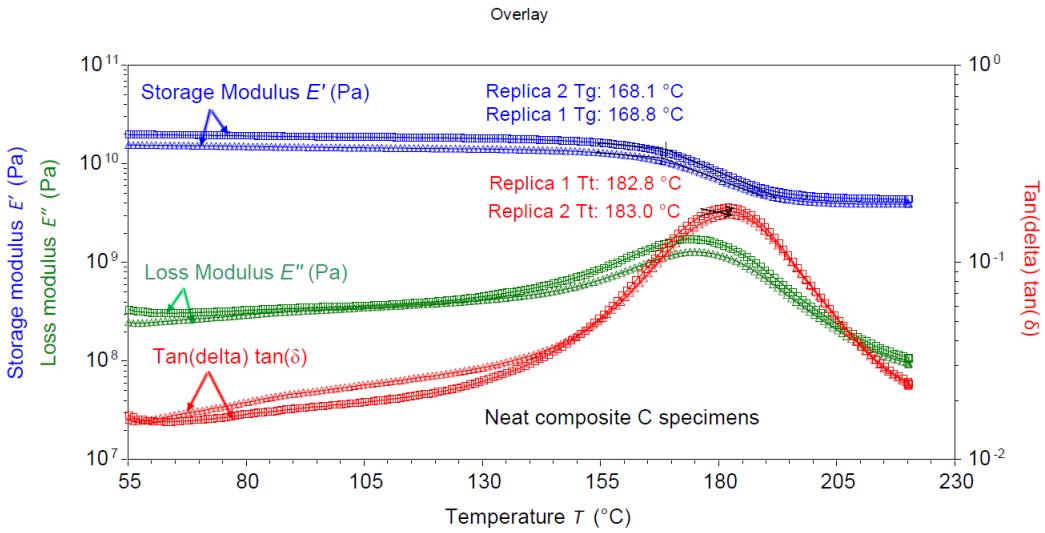

Figure 61. DMA results for two neat composite C specimens.

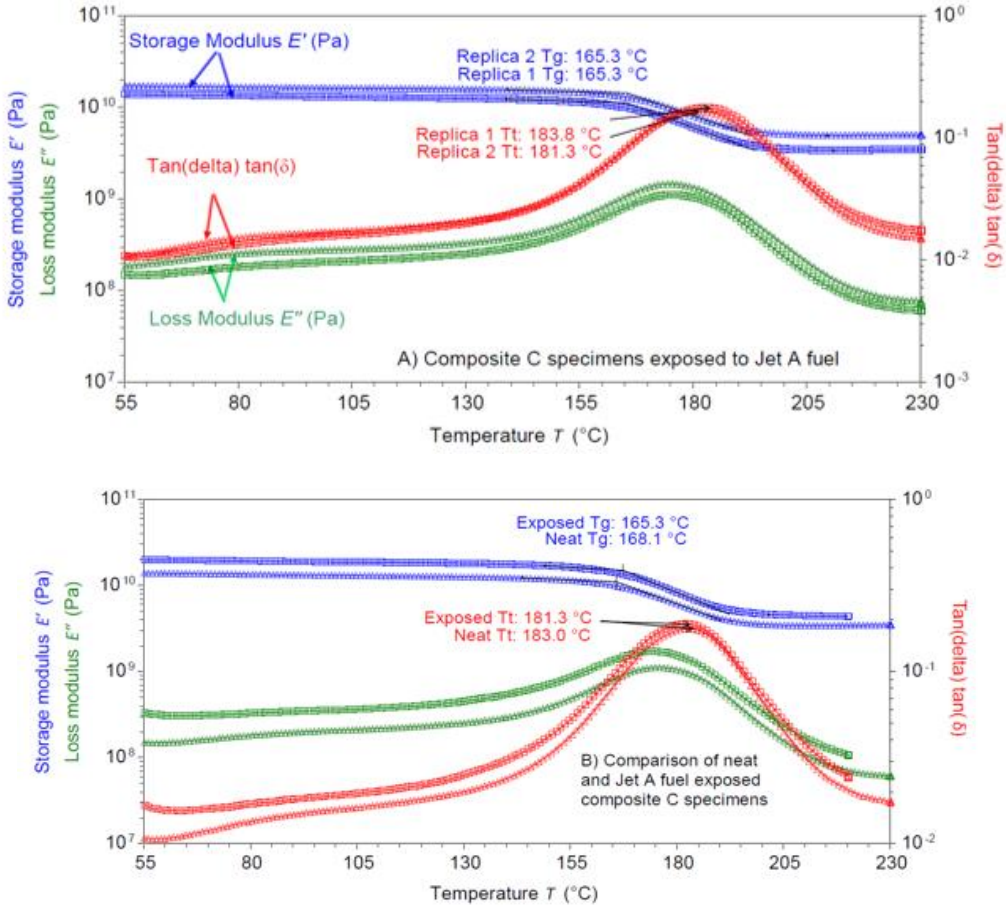

Figure 62. A) DMA results of composite C specimens immersed in Jet A fuel for 700 hours and B) a comparison of one neat and one fuel-exposed composite C specimen.

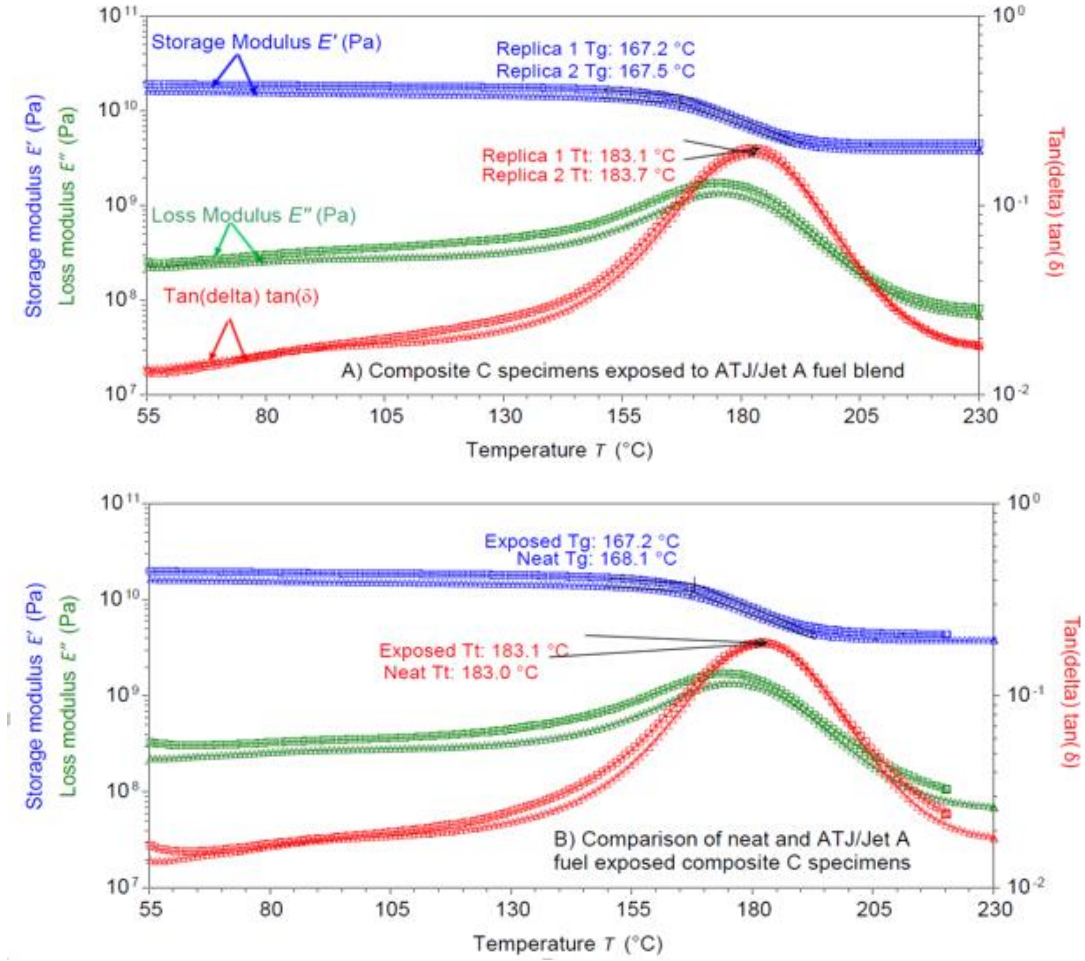

Figure 63. A) DMA results of composite C specimens immersed in ATJ/Jet A blend. (B) Comparison of one neat and one exposed composite C specimen

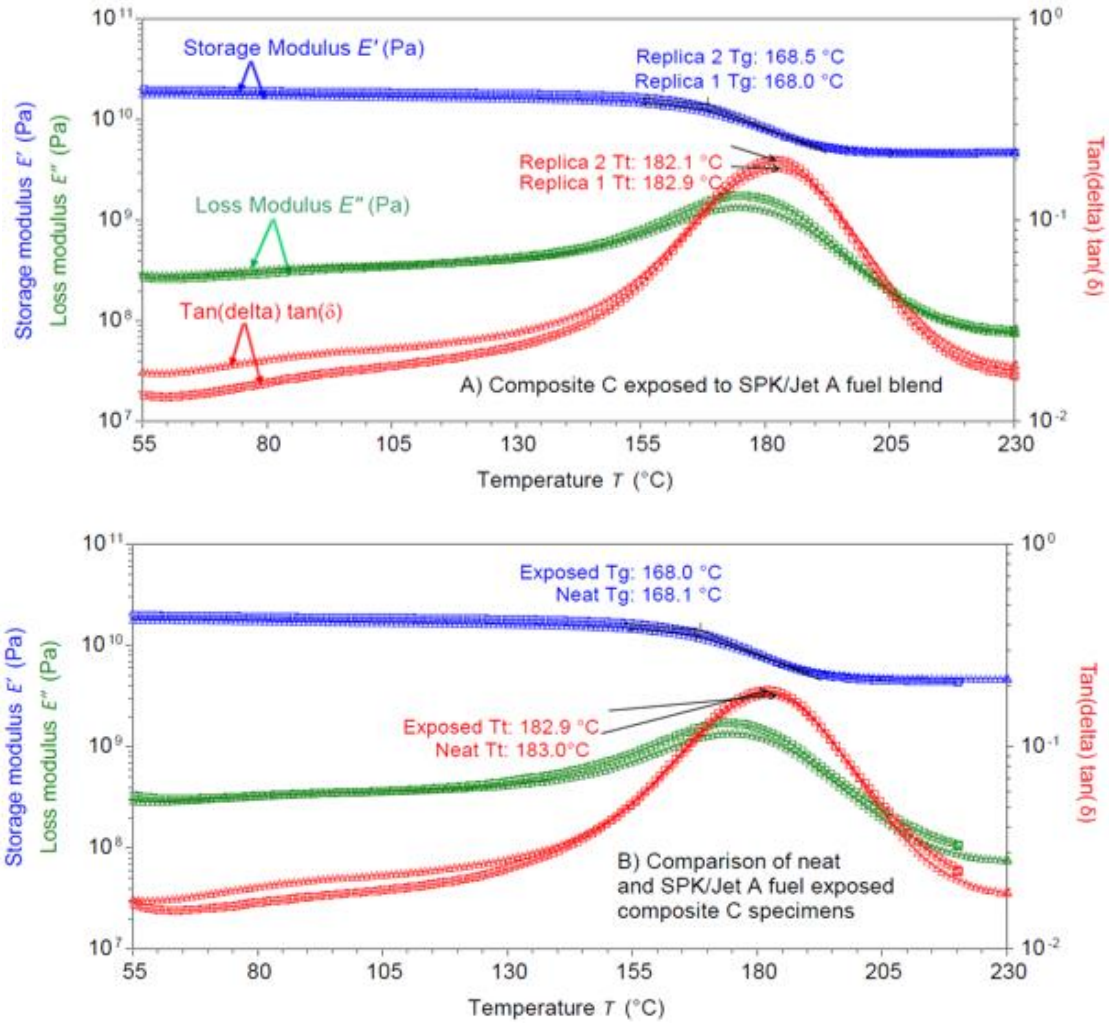

Figure 64. A) DMA results of composite C specimens immersed in SPK/Jet A blend. (B) Comparison of one neat and one exposed composite C specimen.

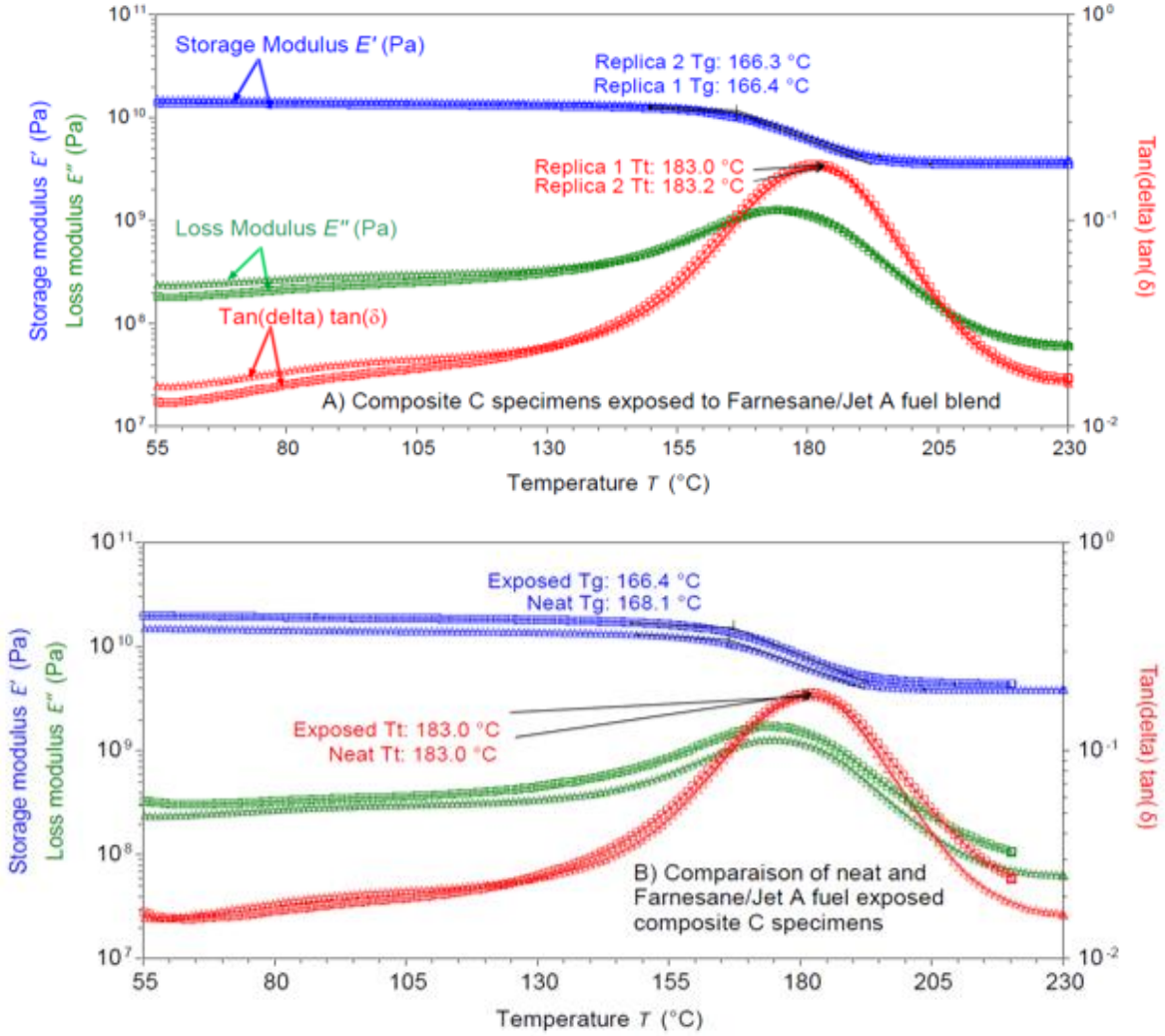

Figure 65. A) Dynamic Mechanical Analysis results of composite C specimens immersed in Farnesane/Jet A blend for 700 hours and B) a comparison of one neat and one fuel-exposed composite C specimen.

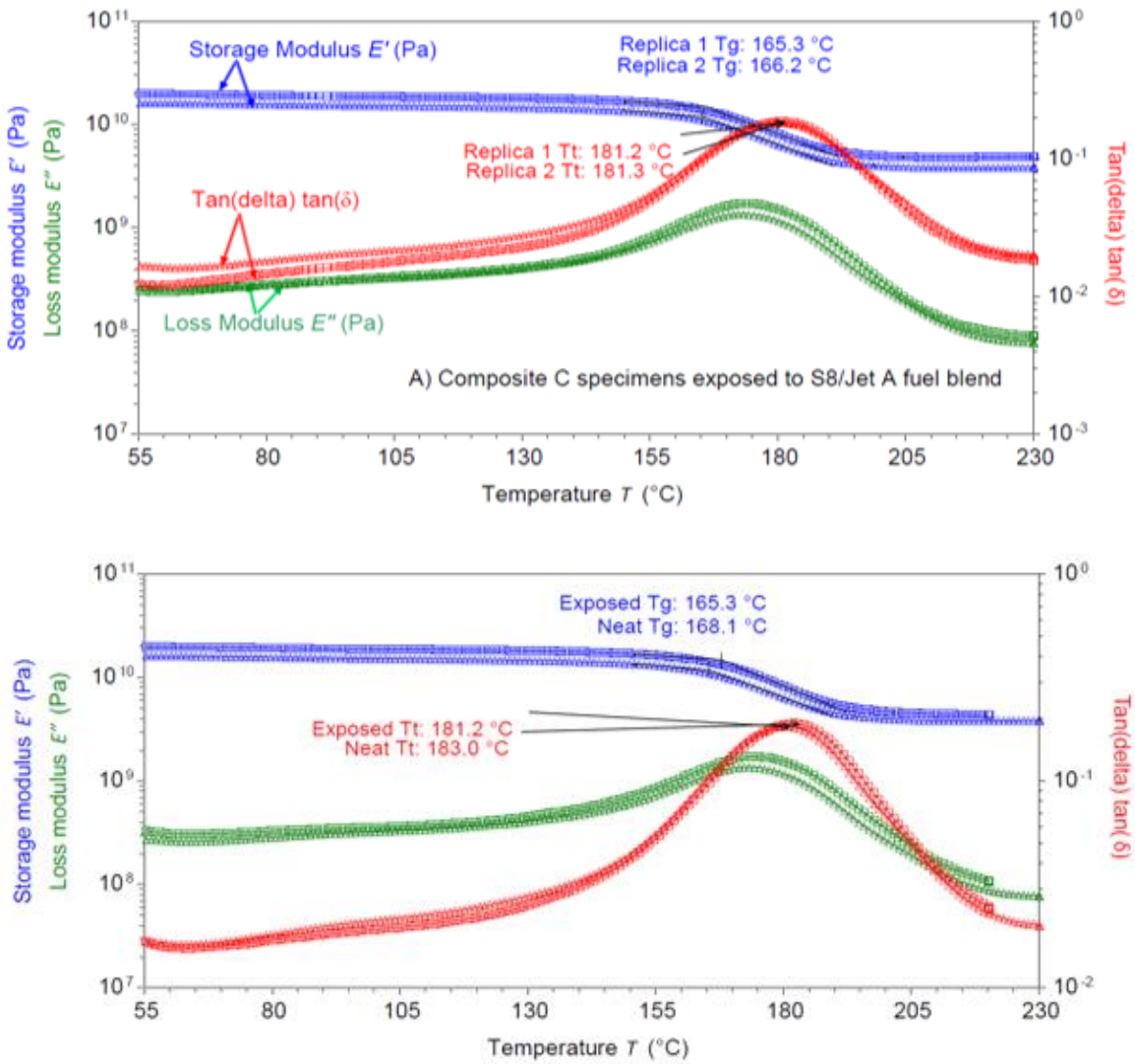

Figure 66. A) DMA results of composite C specimens immersed in S8/Jet A blend for 700 hours and B) a comparison of one neat and one fuel-exposed composite C specimen.

Table 15. Dynamic Mechanical Analysis results for composite C specimens

Specimen type	**Property**	**Neat / Exposed**		**Exposed to Jet A**	**Exposed to ATJ/Jet A blend**	**Exposed to SPK/Jet A blend**	**Exposed to Farnesane /Jet A blend**	**Exposed to S8/Jet A**
C	**DMA T_g (°C)**	**Neat**	**Average ± Standard Deviation**	168.4 ± 0.5	168.4 ± 0.5	168.4 ± 0.5	168.4 ± 0.5	168.4 ± 0.5
			Range (low-high)	168.1 - 168.8	168.1 - 168.8	168.1 - 168.8	168.1 - 168.8	168.1 - 168.8
		Fuel-Exposed	**Average ± Standard Deviation**	165.3 ± 0	167.3 ± 0.2	168.2 ± 0.3	166.3 ± 0.1	165.7 ± 0.6
			Range (low-high)	165.3 – 165.3	167.2 – 167.5	168 – 168.5	166.3 – 166.4	165.3 – 166.2
	Tangent delta (δ) peak T_t (°C)	**Neat**	**Average ± Standard Deviation**	182.9 ± 0.1	182.9 ± 0.1	182.9 ± 0.1	182.9 ± 0.1	182.9 ± 0.1
			Range (low-high)	182.8 - 183	182.8 - 183	182.8 - 183	182.8 - 183	182.8 - 183
		Fuel-Exposed	**Average ± Standard Deviation**	182.55 ± 1.8	183.4 ± 0.4	182.5 ± 0.5	183.1 ± 0.1	181.2 ± 0.1
			Range (low-high)	181.3-183.8	183.1 – 183.7	182.1 – 182.9	183 – 183.2	181.2 – 181.3

5 Conclusions

In recent years, there has been a surge in composite materials usage due to several advantages, primarily due to their enhanced mechanical properties (stiffness, strength, etc.) and tailorability. Despite these benefits, composites may exhibit severe degradation of mechanical and thermomechanical properties under extreme hygrothermal conditions. Moreover, the composite chemical structure may be adversely affected by exposure to and absorption of organic fluids, such as fuels. It is, therefore, important to aircraft flight safety to carefully evaluate property changes as a function of fuel exposure. To reduce the environmental and financial impact of commercial aviation jet fuels, the FAA has recently approved several bio-based jet fuels. However, there is a lack of literature on the impact of bio-based jet fuels on composites. These alternative fuels are obtained through one the following processes: ATJ-SPK, HEFA-SPK, FT-SPK, and HFS-SIP. Therefore, the goal of the present research is to examine the underlying mechanisms behind the glass transition temperature T_g degradation of composite materials when exposed to or immersed in Jet A, 50/50 Gevo ATJ/Jet A50/50 SPK/ Jet A, 50/50 S8/ Jet A, and 20/80 Amyris Farnesane/ Jet A fuels. Different carbon-epoxy and graphite epoxy 2 x 0.5 in^2 specimens with different curing cycles, layups, and thicknesses were used in this study. Vacuum drying was used to remove any remaining moisture in composite specimens before exposing them to the various fuels. Each fuel-exposed specimen was periodically measured during fuel immersion to evaluate mass gain and when fuel uptake saturation occurred. The changes in weight for all these specimens were tracked and illustrated in figures in terms of percentage weight-gain vs time (hours). After a final weighing, fuel-saturated specimens used in DMA following the proper ASTM standard to investigate of fuel absorption effect on T_g. Overall, the fuel uptake and DMA results were well within previous literature findings and results, indicating that the fuel blends used in this study are suitable for use in larger aircraft structures, and perhaps at higher alternative fuel blending ratios.

6 Recommendations for future work

- Explore multiple composite configurations (number of plies, fiber orientation, etc.), with different types of thermoset resins and curing conditions (oven-cure vs. autoclave-cure) relevant to fuel containment systems. Consider both thick and thin samples. Investigate diffusion into a cured epoxy with no fibers. This will allow the delineation of the matrix and fiber contributions on the soaking behavior and indication of a potential change in the mechanical properties of composites.
- Additionally, perform chemical analysis of the different types of fuel in which the specimens are immersed to further understand the effect of pre-existing anomalies in specimens, the nature of matrix crosslinking, and fuel-and-matrix interaction on immersed specimens' weight gain.
- In addition to DMA, conduct other types of matrix-dominated mechanical testing (e.g., compression testing) on all neat and fuel-immersed specimens.
- Investigate multiple soaking and drying cycles and their effects on the mechanical properties for different types of composites.
- Perform computational modeling of the diffusion process in composites using Finite Element Analysis (FEA) software to better understand the effect of the specimen's geometry on the composite' diffusion.

7 References

AOPA. (2016, April 14). *Five Jet Biofuels Now Approved, FAA Says.* Retrieved 2018, from www.aopa.org/news-and-media/all-news/2016/april/14/five-jet-bio-fuels-now-approved-says-faa

ASTM International. (2011). ASTM D7566-11a, Standard Specification for Aviation Turbine Fuel Containing Synthesized Hydrocarbons. *ASTM 2008 Annual Book of Standards*.

ASTM International. (2012). ASTM D4054-09, Standard Practice for Qualification and Approval of New Aviation Turbine Fuels and Fuel Additives. *ASTM International West Conshohocken, PA*. Retrieved from https://www.astm.org/d4054-09.html

ASTM International. (2012). D5229/D5229M-12" Standard Test Method for Moisture Absorption Properties and Equilibrium Conditioning of Polymer Matrix Composite Materials.".

ASTM International. (2013). ASTM D6415 / D6415M - 06a, Standard Test Method for Measuring the Curved Beam Strength of a Fiber-Reinforced Polymer-Matrix Composite. doi:0.1520/D6415_D6415M-06AR13

ASTM International. (2014). ASTM D1665-98, Standard Test Method for Engler Specific Viscosity of Tar Products.

ASTM International. (2015). ASTM D7028 - 07, Standard test method for glass transition temperature (DMA Tg) of polymer matrix composites by dynamic mechanical analysis (DMA).

ASTM International. (2020). D1655-20c, Standard Specification for Aviation Turbine Fuels.

ATAG. (2009, May). Beginners Guide to Aviation Biofuels. Switzerland. Retrieved from https://www.verifavia.com/bases/ressource_pdf/124/BeginnersGuide-Biofuels-WebRes.pdf

Aviation Maintenance Technician Handook - Airframe, Volume 2. (2018). *FAA-H-8083-31A*. U.S. Department of Transportation Federal Aviation Administration. Retrieved from https://www.faa.gov/regulations_policies/handbooks_manuals/aviation/media/amt_airframe_hb_vol_2.pdf

Baeza, A.-l., Maria, A., Llamas Lois, A., Bolonio Martin, D., Canoira Lopez, L., Sanz Perez, F., & Lapuerta , M. (2014). Airplane materials compatibility with blends of fossil kerosene

jet A1 with biokerosenes from babassu, palm kernel and coconut oils. *Global nest journal, 16*(6), 1066-1075.

Bassou, R., Harich, N., Kundu, S., Priddy, M. W., Lacy, T. E., & Pittman, C. U. (2019). *DOT/FAA/TC-20/22 - Effect of Jet Fuels Exposure on Aerospace Composites - Literature Review.* Federal Aviation Administration. Atlantic City International Airport, NJ: FAA William J. Hughes Technical Center. Retrieved from https://rosap.ntl.bts.gov/view/dot/57829

Bassou, R., Harich, N., Lacy, T., Pittman, C., Priddy, M. W., & Kundu, S. (2021). *DOT/FAA/TC-20/22 - Effect of Jet Fuels Exposure on Aerospace Composites - Literature Review.* Washington, D.C.: U.S. Department of Transportation.

Biofuels for Aviation: Technology Brief. (2017). Retrieved 2018, from http://www.irena.org/documentdownloads/publications/irena_biofuels_for_aviation_2017.pdf

Bond, D., & Smith, P. (2006). Modeling the transport of low-molecular-weight penetrants within polymer matrix composites. *Applied Mechanics Review, 59*(5), 249-268.

CAAFI Frequently Asked Questions. (n.d.). Retrieved 2019, from www.caafi.org/resources/faq.html

Curliss, D. B. (1991). *The effect of Jet fuel exposure on advanced aerospace composites I: Thermal and Chemical Analysis.* Wright Lab Wright-Patterson AFB OH, USA. Retrieved from https://apps.dtic.mil/sti/pdfs/ADA246559.pdf

Curliss, D., & Carlin, D. (1989). *Effect of jet-fuel exposure on advanced aerospace composites, II: Mechanical properties. Final report.* Air Force Wright Research and Development Center , Wright-Patterson AFB, OH (USA).

Defense Standard. (2002). 91-91/4: Turbine Fuel. *Aviation Kerosine Type, A-1 NATO code: F-35 Joint Service Designation: AVTUR.*

Edwards, J., Shafer, L., & Klein, J. (2012). *US Air Force Hydroprocessed Renewable Jet (HRJ) Fuel Research.* AIR FORCE RESEARCH LAB WRIGHT-PATTERSON AFB OH PROPULSION DIRECTORATE/TURBINE ENGINE DIVISION.

Fellet, M. (2016, September 19). *Now Boarding: Commercial Planes Take Flight with Biobased Jet aFuel.* Retrieved 2018, from Chemical and Engineering News (C&EN): cen.acs.org/articles/94/i37/boarding-Commercial-planes-take-flight.html

Graham, J. (2011). Impact of Alternative Jet Fuel and Fuel Blends on Non-Metallic Materials Used in Commerical Aircraft Fuel Systems. *Federal Aviation Administration and The Boeing Company, Technical Report DTFAWA-10-C-0030*.

Horn, W., Soeganto, A., & Shaikh, F. (1989). Degradation of mechanical properties of advanced composites exposed to aircraft environment. *AIAA journal, 27*(10), 1399-1405.

La Saponara, V. (2011). Environmental and chemical degradation of carbon/epoxy and structural adhesive for aerospace applications: Fickian and anomalous diffusion, Arrhenius kinetics. *Composite Structures, 93*(9), 2180-2195.

Landry, B., LaPlante, G., & LeBlanc, L. (2012). Environmental effects on mode II fatigue delamination growth in an aerospace grade carbon/epoxy composite. *Composites Part A: Applied Science and Manufacturing, 43*(3), 475-485.

Loos, A., & Springer , G. (1979). Moisture absorption of graphite-epoxy composites immersed in liquids and in humid air. *Journal of Composite Materials, 13*(2), 131-147.

Ma, C.-C., Lee, C.-L., & Tai, N.-H. (1992). Chemical resistance of carbon fiber-reinforced poly (ether ether ketone) and poly (phenylene sulfide) composites. *Polymer Composites, 13*(6), 435-440. doi:https://doi.org/10.1002/pc.750130606

Mazumdar, S. (2001). *Composites manufacturing: Materials, Product, and Process Engineering.* CRC Press.

Menard, K., & Menard, N. (2002). Dynamic Mechanical Analysis in the Analysis of Polymers and Rubbers. doi:10.1002/0471440264.pst102.pub2

Michel, J. (2016). *Work Package 5, D5. 2: Final Report on Technical Compatibility, Certification and Deployment.* Work Package, CORE-JetFuel. Retrieved from https://www.senasa.es/recursos/adobePDF/2018/pdf/core-jet-fuel/5_2GA_605716_CORE-JetFuel_Deliverable_5.2_Final%20_Report_on_Technical_Com.pdf

Moses, C., & Roets, P. (2009). Properties, characteristics, and combustion performance of sasol fully synthetic jet fuel. *Journal of Engineering for Gas Turbines Power*. doi:10.1115/1.3028234

New alternative jet fuel approved. (2016, April 14). (FAA) Retrieved 2018, from Federal Aviation Administration: https://www.faa.gov/news/updates/?newsId=85425

Pires, A., Han, Y., Kramlich, J., & Garcia-Perez, M. (2018). Chemical composition and fuel properties of alternative jet fuels. *BioResources.com, 13*(2), 2632-2657. Retrieved from https://ojs.cnr.ncsu.edu/index.php/BioRes/article/view/BioRes_13_2_2632_Pires_Chemical_Composition_Fuel_Properties_Jet/5919

Pond & Company, Inc. (2012). *Investigative Study to Determine Effects of Hydro-Treated Renewable JP-8 Jet Fuel Blend in Existing Fuels Infrastructure.* Retrieved from https://apps.dtic.mil/sti/pdfs/AD1030329.pdf

Rahmes, T., Kinder, J., Crenfeldt, G., LeDuc, G., Abe, Y., McCall, M., . . . Lewis, C. (2009). Sustainable bio-derived synthetic paraffinic kerosene (Bio-SPK) jet fuel flights and engine tests program results. *9th AIAA aviation technology, integration, and operations conference (ATIO) and aircraft noise and emissions reduction symposium (ANERS)*, (p. 7002). doi:10.2514/6.2009-7002

Sala, G. (2000). Composite degradation due to fluid absorption. *Composites Part B: Engineering, 31*(5), 357-373.

Soloiu, V., Muinos, M., Harp, S., Naes, T., & Gaubert, R. (2016). *Combustion and Emissions Characteristics of Dual Fuel Premixed Charge Compression Ignition with Direct Injection of Synthetic FT Kerosene Produced from Natural Gas and Port Fuel Injection of n-Butanol.* SAE World Congress and Exhibition Technical Paper. doi:10.4271/2016-01-0787

Sugita, Y., Winkelmann, C., & La Saponara, V. (2010). Environmental and chemical degradation of carbon/epoxy lap joints for aerospace applications, and effects on their mechanical performance. *Composites Science and Technology, 70*(5), 829-839.